NANOINDENTATION TESTING OF PORCINE BONE

by

YuSheng Chang

B.S. in Mechanical Engineering, National Taiwan University, 2010

Submitted to the Graduate Faculty of

Swanson School of Engineering in partial fulfillment

of the requirements for the degree of

Master of Science in Mechanical Engineering

University of Pittsburgh

2014

UNIVERSITY OF PITTSBURGH

SWANSON SCHOOL OF ENGINEERING

This thesis was presented

by

YuSheng Chang

It was defended on

June 6th, 2014

and approved by

Patrick Smolinski, Ph.D., Associate Professor

Department of Mechanical Engineering and Material Science

William S. Slaughter, Ph.D., Associate Professor

Department of Mechanical Engineering and Material Science

Mark Miller, Ph.D., Associate Professor

Department of Mechanical Engineering and Material Science

Thesis Advisor: Patrick Smolinski, Ph.D. Associate Professor

Department of Mechanical Engineering and Material Science

NANOINDENTATION TESTING OF PORCINE BONE

YuSheng Chang, M.S.

University of Pittsburgh, 2014

Nanoindentation testing is a technique that is used to measure mechanical properties of materials at the nano-scale. The method has been used to measure properties of metals, ceramics and also biological materials. In this study nanoindentation testing was used to measure the reduced modulus and hardness in the porcine tibia and femur. Testing was done to measure the properties in different directions and also in the anterior and posterior regions of the bone. Two bone samples were analyzed in this study. Bone samples were obtained and cleaned and polished in the area of interest. Samples were tested after air drying for 48 hours. Digital microscopy was used to locate osteon bone in the region of interest. The bone was testing in the axial (x) direction, sagittal plane (y) direction and the frontal plane (z) direction. A loading function with a 5 s rise time, 5 s holding time and 5 s unloading time with a peak value of 4000 µN was used. Statistical analysis of the data was done using a one-way Anova, Tukey test and a linear mixed model.

In the first sample, mechanical properties did not vary in different areas tested within a region while in the second sample properties did vary between areas in some regions. Differences in mechanical properties between anterior and posterior regions were found in both femur and tibia of the first sample and the femur of the second sample. Besides, differences in mechanical properties in the different directions were found in both the tibia

and femur with most of the axial direction being highest and those in the sagittal plane being the lowest. In general the properties in the femur were greater than that of the tibia.

Greater loading in certain bone regions may induce higher hardness and elastic modulus. The different properties in the different directions may suggest a plywood-like composite structure with most fibers orthogonal to the laminate direction. The evaluation of bone mechanical properties can contribute to the knowledge of the effects of location, disease or other factors on the tissue.

TABLE OF CONTENTS

LIST OF TABLES

LIST OF FIGURES

PREFACE

It is a great opportunity to have such a research experience. Gratefully thank Professor Patrick Smolinski for his advising. I would also like to thank Hsin-Wen Chang for her help in statistical analysis. Thanks Monica Linda-Rosen, JunJun Zhu and Brandon Marshall for their support through this period of time.

1.0 INTRODUCTION

1.1 NANOINDENTATION HISTORY

There is a long history of the use of indentation testing to measure material hardness. Techniques such as Rockwell and Vickers methods have been developed to measure and characterize this material property. The basic idea is to press an indenter into a material with known force and measure the distance that the indenter penetrates into the material. Based on derived formulas, a hardness number is calculated, e.g. 10000HV for diamond in Vickers test. This number represented the material property for a particular test and can be converted to other measurements.

With the advance of technology, the testing scale has been decreased to submicron-scale, or even nano-scale. Nanoindentation, also known as instrumented indentation or depth-sensing indentation, has been developed over the past decade and has advantages because of its accuracy among different materials and its capability of testing the material in the depth range of few nanometers. In addition, it can be used to test a small, localized area which is important for thin coatings or inhomogeneous materials composed of different grains or crystals.

The principle is to measure the force and displacement, and calculate the projected contact area of the material induced by a tip. The hardness (H) and reduced modulus (Er) can be directly obtained and the elastic modulus (E) can be further computed [17, 52-55]. Equation (1) gives the relation between elastic modulus and reduced modulus,

$$\frac{1}{E_r} = \frac{(1-v^2)}{E} + \frac{(1-v_i^2)}{E_i} \qquad (1)$$

where υ is the Poisson's ratio of the indented material and υ_i and E_i are the Poisson's ratio and elastic modulus of the indenter tip [52].

1.2 TESTING MATERIALS

Nanoindentation has been applied to many different types of materials including crystal materials [14], thin films [22] and ceramics [24]. It has also been proved a useful method for understanding structure and properties of the biological tissues and providing information for developing biomaterials [3, 8, 19]. Due to their complexity, variability and ability to change, that the mechanical properties of the biological tissues can be affected by other factors, there has been considerable interest in these materials.

Biological materials can be roughly divided into two groups: hard and soft materials. Common hard biological materials are bone [21] and tooth [25]. Soft biological materials are vascular tissue [4], tendon etc. Efforts have been made to deal with the particular testing problems of the soft tissue such as surface detection, adhesion and drifting, which can cause errors in measurement [2, 5, 13].

1.3 OTHER STUDIES

Some studies have been done for comparing the differences in equipment. For instance, Paietta, Campbell and Ferguson varied the indenter tip radius in measuring bovine femoral cortical bone to see the effect of tip size on the mechanical properties. The sample was embedded in methylmethacrylate and polished to a 0.25 μm finish. Spherical indentation tips

with radii from 5, 25, 65 to 200 µm were used and the loading was set to achieve the desired displacement, ranging from 100 to 2000nm, with the same loading and unloading rate of 0.5 mN/s and dwell time of 120 seconds. They found that for contact depth smaller than 500 nm, the reduced modulus decreased with the increasing of the tip size. With smaller radius tips (5 and25 µm) and for the contact depth of 0-500 nm, there was more scatter in the modulus data, while the larger tip radius (65 and 200 µm) showed more uniform results (Figure 1). For the 5 µm radius tip, the reduce modulus (Er) increased with the contact depth (0-2000 nm) while the variability decreased (Figure 2). The conclusion was that the modulus measured from shallow indent with smaller tip radius can be compared to the modulus from the larger tip radius [18].
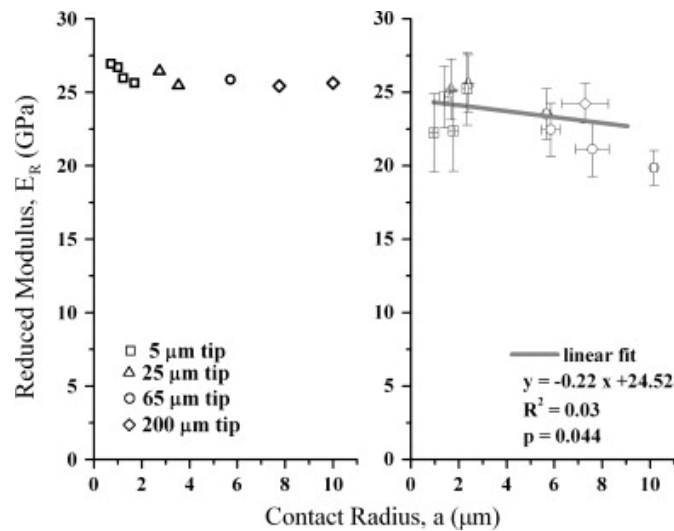
Figure 1: Plot on the left showing the finite element analysis result for reduced modulus with different tip sizes. Plot on the right showing the experimental data for reduced modulus with different tip sizes [18].
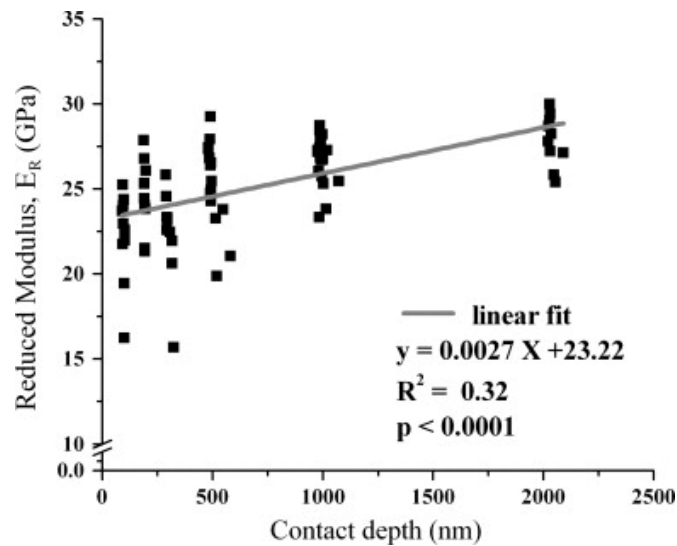
Figure 2: Reduced modulus variation with indent depth for the 5 µm radius tip [18].

Besides the hardness and elastic modulus, the viscoelastic behavior of the materials can also be measured by nanoindentation. Wu et al. tested bovine femoral cortical bone under different loading rates and holding times. They used the data to fit three models: the standard linear solid, the Burgers model and the two-dashpot Kelvin model. The bone was polished using successive grit papers and aluminum suspension to a 0.25 µm finish. A Berkovich pyramidal tip (Figure 3) was used to indent the bone with a maximum force 10 mN and loading/ unloading rates 2 mN/s. They found that the best model for predicting the long-term viscosity of the bone tissue was the Burgers model (Figure 4) [23].

Isaksson et al. investigated the loading protocols that can best acquire the viscoelasticity properties of the bone [12]. Protocols included creep behavior, load-rate sensitivity, dissipated energy and semi-dynamic test methods (Figure 5). The creep behavior method alters the dwell time; the rate sensitivity test changes the loading rate; the dissipated energy method uses repeated cyclic loading whereas the semi-dynamic test incorporates the dynamic loading function into the quasi-static loading function. The

samples were cortical bone from the bovine distal femur and the trabecular bone from the proximal tibia. Silicon carbide papers (500, 800, 1000, 1200 and 4000 grid) were used to polish the sample under deionized water to achieve a 55 nm average surface roughness. The indenter was equipped with a cube corner diamond tip that had a 40 nm radius. The results showed that depending on the methods and the loading factors such like loading rate, holding time etc., the coefficient of variation for the reproducibility of each method varied from 9-40%. In addition, the semi-dynamic method under high frequency dynamic loading had the lowest 9-10% coefficient of variance, indicating that this protocol had the best consistency for measuring viscoelasticity properties [12].

In conclusion, researchers have been using nanoindentation to test different kinds of materials including crystal material, ceramics, thin film, biological materials, etc. This technique has been employed in not only measuring hardness and elastic modulus, but also characterizing the viscoelasticity. Scientists have also investigated the factors that may alter the experimental result such as loading protocol and differing tips. It can be seen that in the future, there will be more exploration and application for this technique.
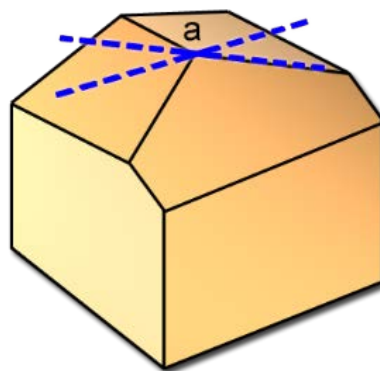
Figure 3: A three-sided pyramidal Berkovich tip shown on the Hysitron website

(http://www.hysitron.com/Default.aspx?tabid=120).
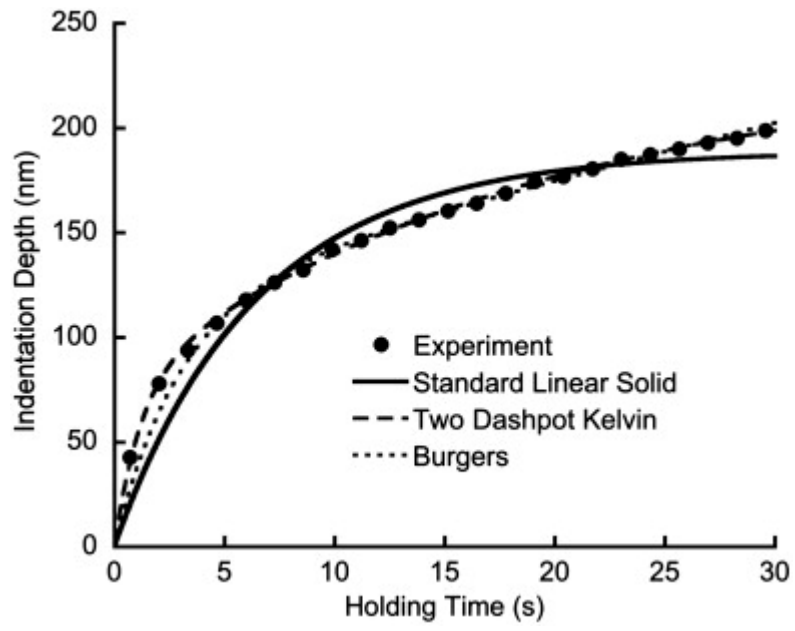
Figure 4: Experimental data set with three models curve fits [23].
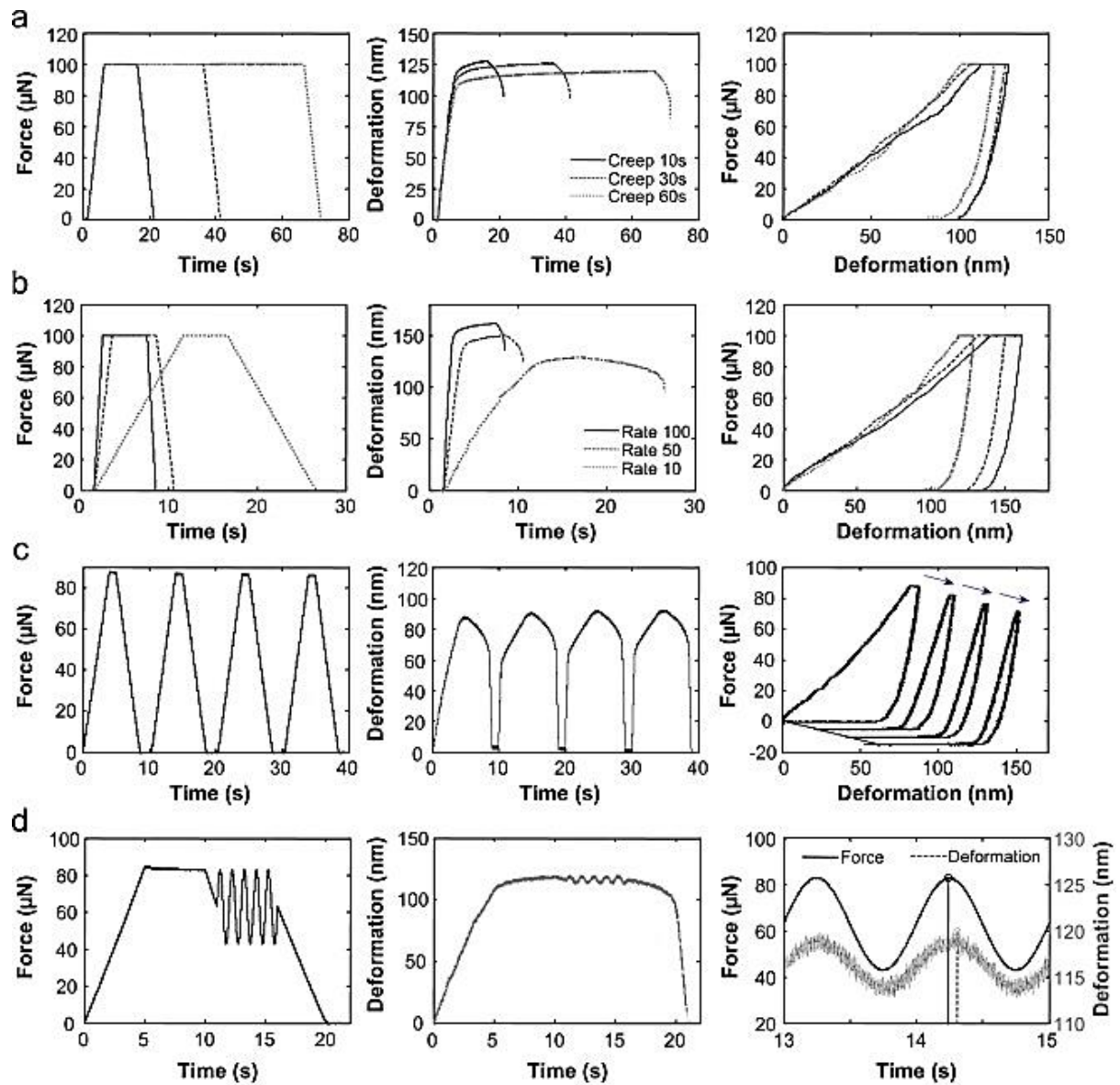
Figure 5: Loading protocols (left) with the displacement-time curves (middle) and loading-displacement curves (right). (a) The creep behavior method. (b) The load-rate sensitivity method. (c) The dissipated energy method. (d) The semi-dynamic test method [12].

2.0 BACKGROUND

2.1 NANOINDENTATION ON THE BONE

Bone tissue is of interest to many scientists not only because of its crucial character for human daily life, but also its hierarchical structure and anisotropic property. In addition, the material property of the bone can be altered by external factors such as drugs, loading or aging. Rho et al. described the hierarchical structure of the bones and schematically illustrated the different scales of the bone tissue (Figure 6).
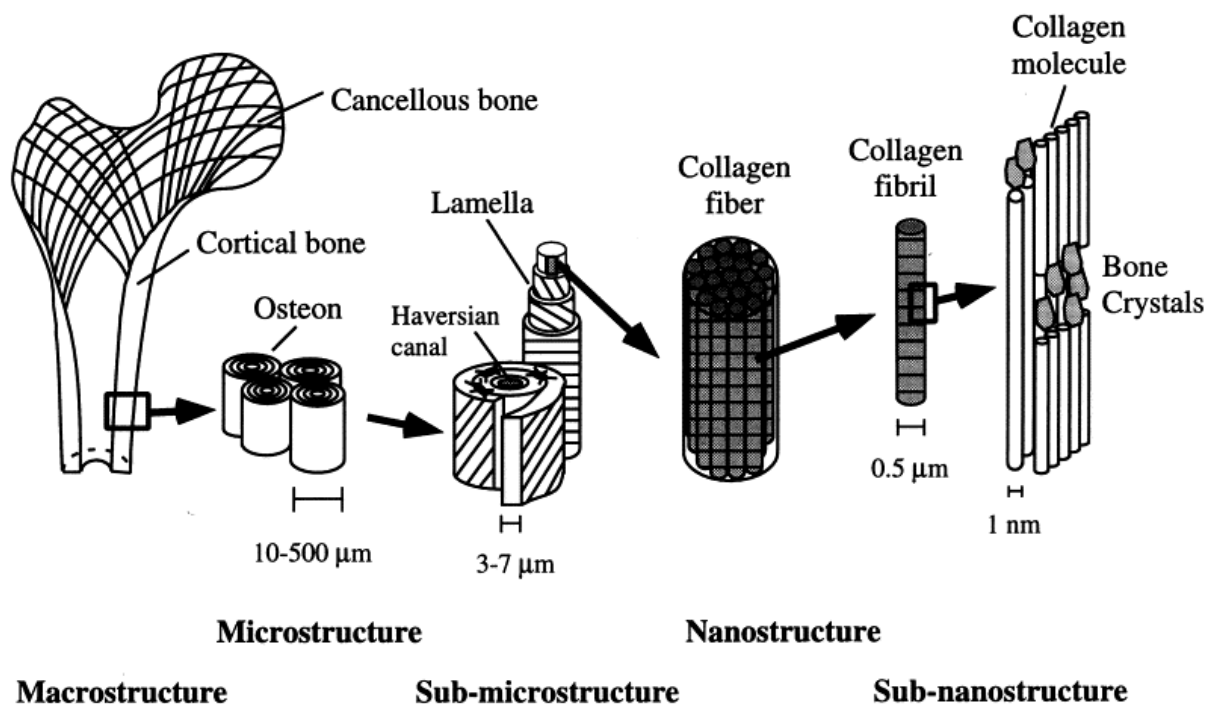
Figure 6: Hierachical structure of the bones [20].

The study of the spatial variation in material properties in bone has been one of the most popular research areas. It has been proposed that bone may develop inhomogeneous mechanical properties due to stress variations between regions. Giambini et al. tested the trabecular bone longitudinally from human vertebral sections T7, T8 (Thoracic) and L4 (Lumbar). The samples were prepared by polishing with grit papers followed by 0.05 µm aluminum powder. Samples were left dry. The loading rate was a constant 333 µN/s and the maximum force was 1 mN with a five seconds dwell time. The study showed that there was no significant spatial difference in elastic modulus or hardness in the posterior regions of the T7, T8 and L4 vertebrae. Besides, no differences were found within each section, e.g. properties in T7 were the same for the anterior and posterior regions. However, they found that modulus and hardness were statistically higher in the anterior regions of T7 (E: 19.8 ± 1.3 GPa, H: 0.74 ± 0.07 GPa) and T8 (E: 19.6 ± 1.4 GPa, H: 0.74 ± 0.04 GPa) compared to L4 (E: 17.6 ± 0.5 GPa, H: 0.64 ± 0.06 GPa) vertebrae. It is the first study that reported the variation of mechanical properties between thoracic and lumbar spine [9].

With bone it may be the case that, even within a small region of sample, the properties and the tissue contents may differ and it has been proposed that the modulus and hardness measured at a local area should correlate to the mineral content in that area. Gupta et al. used a single female femoral cortical bone and compared the differences in mechanical properties and mineral content between osteonal and interstitial bone. The sample was polished with grit papers and diamond grain (down to 1 µm) to achieve an average surface roughness ranging from 25 to 30 nm followed by air drying. One of the loading protocols was that 1000 µN max load reached in five seconds with a dwell time of 60s, followed by unloading to 200 µN in 2.5s, holding for 20s, and then unloading to zero in one second. The representative load function is shown in the Figure 7. Another loading function was similar,

except that the max load was 500 μN and the holding force was 100 μN. These two loading histories were used to cover the indent depth ranging from about 137 nm to about 234 nm, which is similar to the standard fused quartz sample calibration depth. This study showed that modulus and hardness have significant differences between the secondary osteons (~24 GPa to ~27 GPa) and interstitial bone (higher than 30 GPa). However, there were no significant differences in mechanical properties found between three osteons of the cortical bone (Figure 8). Mineral content correlated with both moduli (Figure 9). The study proposed that the variant properties in osteons and interstitial bone may be a crack-arresting mechanism [11].
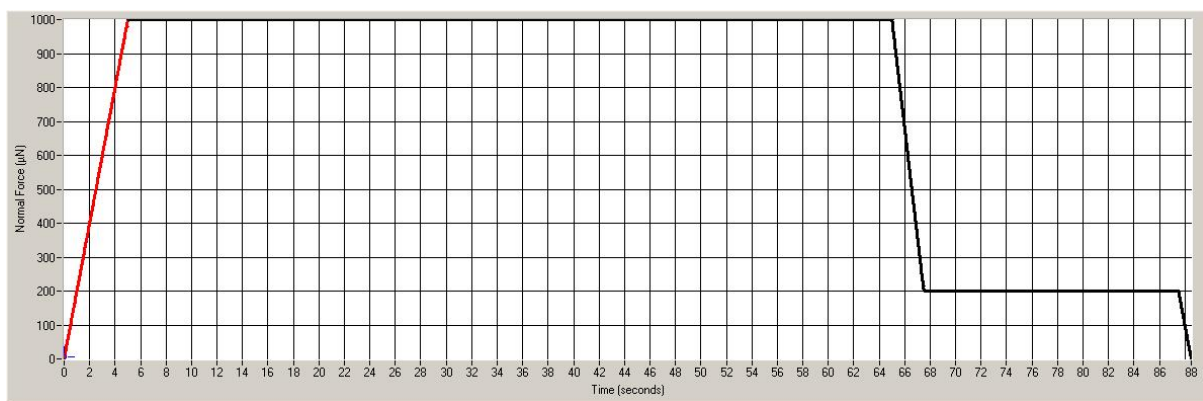
Figure 7: The representative loading function for Gupta et al. study.
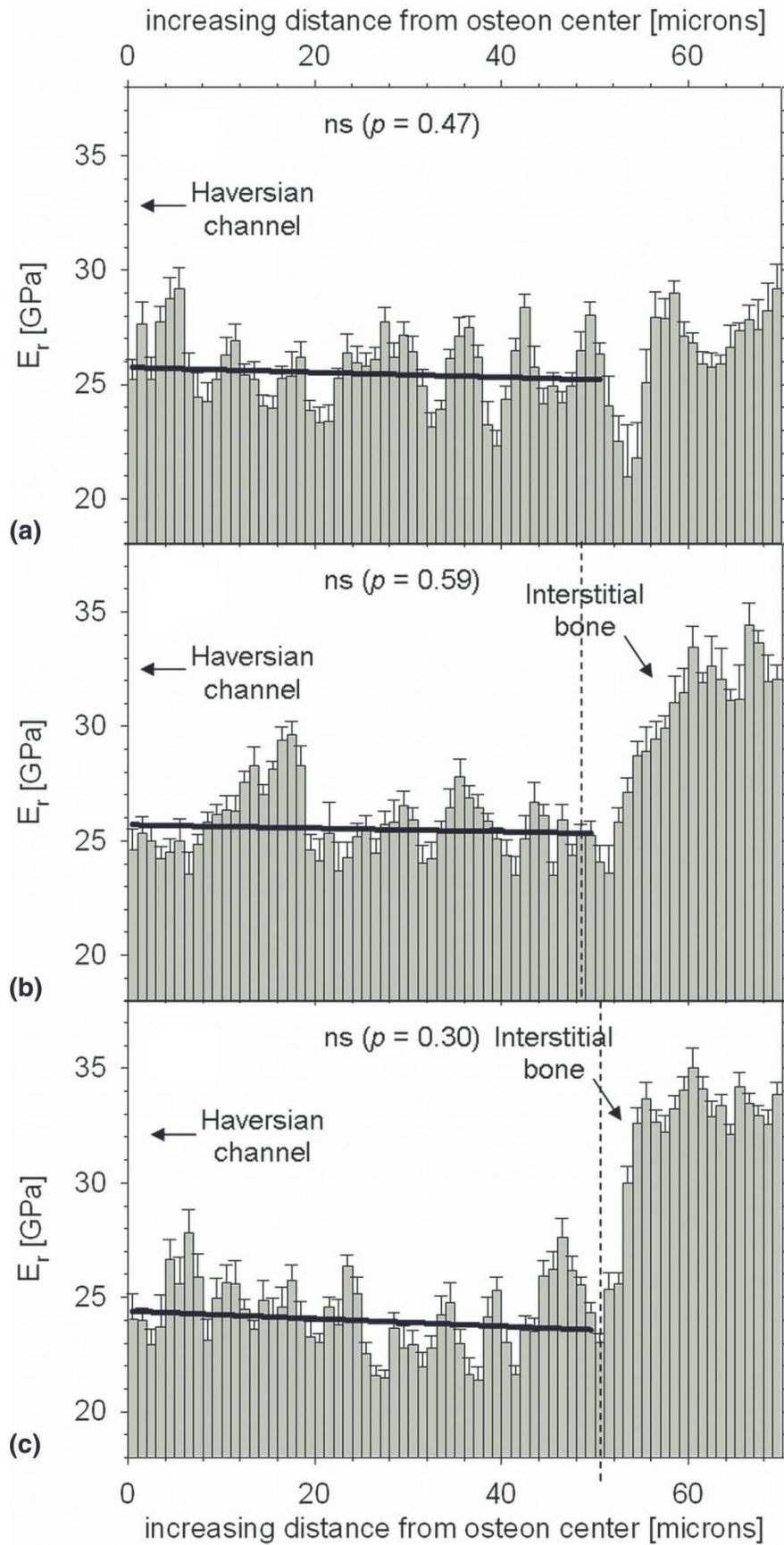
Figure 8: No significant differences for reduced moduli in three osteons (a, b and c) [11].
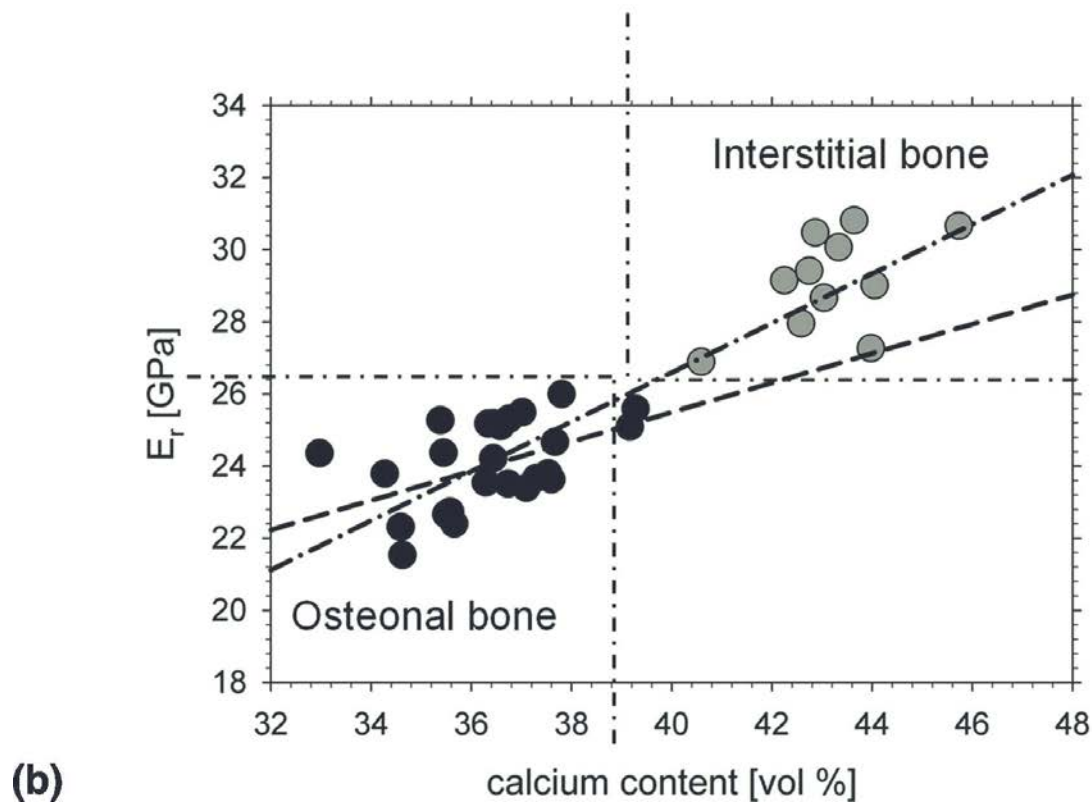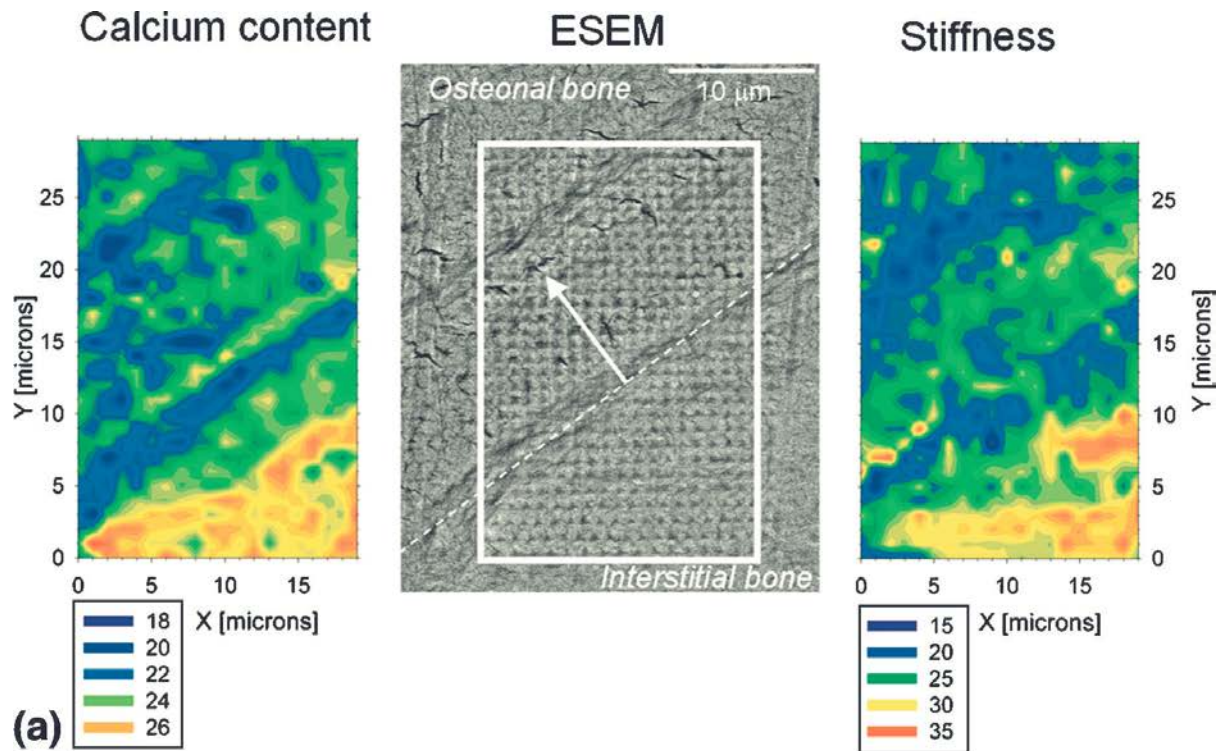
Figure 9: (a) Plot showing stiffness and calcium content. The white arrow and dashed line used to group indent points in the osteonal and the interstitial bone. (b) Plot showing a positive correlation between the reduced modulus and the calcium content [11].

Furthermore, bone material properties may depend on orientation of the sample (anisotropy). Fan et al. examined male tibia cortical bone to investigate the influence of the testing directions. The bone sample was dehydrated through series of alcohol mixtures and fixed in epoxy resin followed by polishing to a 0.05 μm roughness. A maximum load of 8000 μN was selected with a 20 seconds loading segment, resulting in about a 700 nm indent depth. Indentation using a Berkovich tip on twelve orientations was conducted. Besides the three directions based on a Cartesian coordinate system, planes- 30, 45 and 60 degrees away from each axis were chosen as the testing directions (Figure 10). They found significant differences between osteonic and interstitial lamellae in all directions (Figure 11). The results suggested orthogonal mechanical properties. In addition, comparing the corrected result using previously developed models (equation (2) and (3)) by Swadener et al. [27, 28] and Rho et al. [26], they proved the moduli can be quantitatively calculated using the equation [6],

$$M = \frac{4\pi}{\int_0^{2\pi} \frac{a_{3i} B_{ij}^{-1}(\gamma) a_{3j}}{\sqrt{\frac{a_1}{a_2} \cos^2 \gamma + \frac{a_2}{a_1} \sin^2 \gamma}}} \tag{2}$$

where M is the indentation modulus, and a_1/a_2 is the ratio of elliptical axes of the projected area of contact, and B_{ij} is the components of the first Barnett-Lothe tensor, and ϒ is the angle defining the displacement direction at the free surface, and a_{3i} and a_{3j} are the direction cosines of the angle between indent direction and principal direction.

$$M_{mixture} = (CSAF) \times (M_{osteons}) + (1 - CSAF) \times (M_{interstitial}) \tag{3}$$

The constant CSAF, the corrected secondary osteonal area, is 0.388 for human tibia.
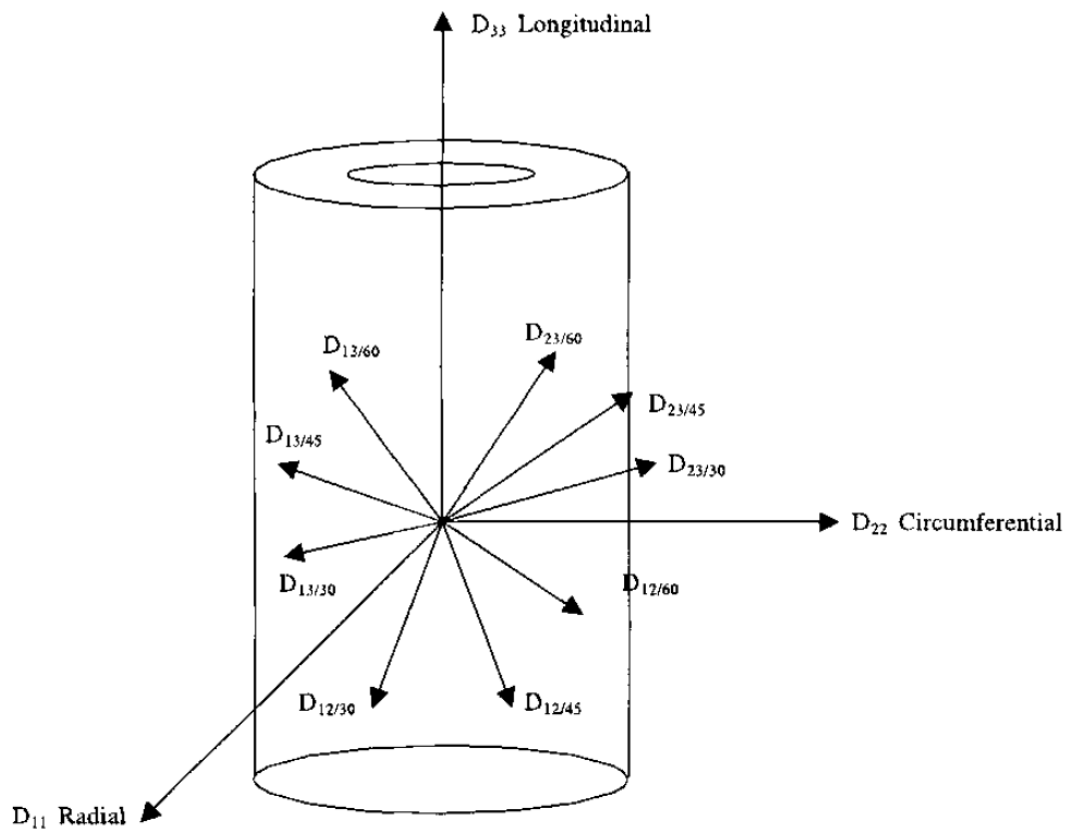
Figure 10: Twelve directions of interest in Fan et al. study [6].

Table 1
Average experimental indentation modulus values (M_{exp}) for osteonic and interstitial lamellae

Indentation directions	Experimental indentation modulus (M_{exp}, GPa), average $\pm$ SD	
	Osteonic lamellae	Interstitial lamellae
D_{11}	16.6 ± 1.5	19.7 ± 1.5
D_{22}	17.0 ± 2.2	18.5 ± 1.1
D_{33}	25.1 ± 2.1	27.1 ± 1.7
$D_{12/30}$	15.7 ± 2.3	20.4 ± 1.8
$D_{12/45}$	16.0 ± 2.0	21.1 ± 1.4
$D_{12/60}$	14.9 ± 2.0	18.9 ± 1.4
$D_{13/30}$	18.4 ± 1.1	20.0 ± 1.4
$D_{13/45}$	18.4 ± 0.9	22.4 ± 1.6
$D_{13/60}$	21.8 ± 2.6	24.8 ± 1.0
$D_{23/30}$	17.6 ± 1.3	20.0 ± 1.4
$D_{23/45}$	18.2 ± 1.4	21.7 ± 1.2
$D_{23/60}$	21.9 ± 2.0	25.2 ± 1.0

Figure 11: The moduli (M_{exp}) measured from the osteonal lamellae all significant lower than those from the interstitial lamellae [6].

Table 2
Corrected experimental (M_{exp}) and predicted (M_{pre}) indentation modulus values for various orientations

Indentation direction	Corrected M_{exp} (GPa) average ± SD	M_{pre} (GPa) average
D_{11}	14.9 ± 0.98	14.0
D_{22}	14.4 ± 0.35	14.5
D_{33}	21.1 ± 1.01	19.7
$D_{12/30}$	14.9 ± 0.96	14.1
$D_{12/45}$	15.4 ± 1.46	14.2
$D_{12/60}$	13.9 ± 1.78	14.4
$D_{13/30}$	15.6 ± 0.89	15.0
$D_{13/45}$	16.7 ± 0.57	16.3
$D_{13/60}$	19.0 ± 0.95	17.8
$D_{23/30}$	15.3 ± 0.48	15.5
$D_{23/45}$	16.3 ± 0.60	16.7
$D_{23/60}$	19.2 ± 1.57	18.0

Corrected M_{exp} data were obtained after a rule of mixture (Eq. (3)) and assuming a 15% increase for dehydration. Predicted M_{pre} values were calculated using elastic stiffness components determined by ultrasound test [10]. (SD: standard deviation.)

Figure 12: The corrected modulus from Eq.(3) and the predicted modulus [6].
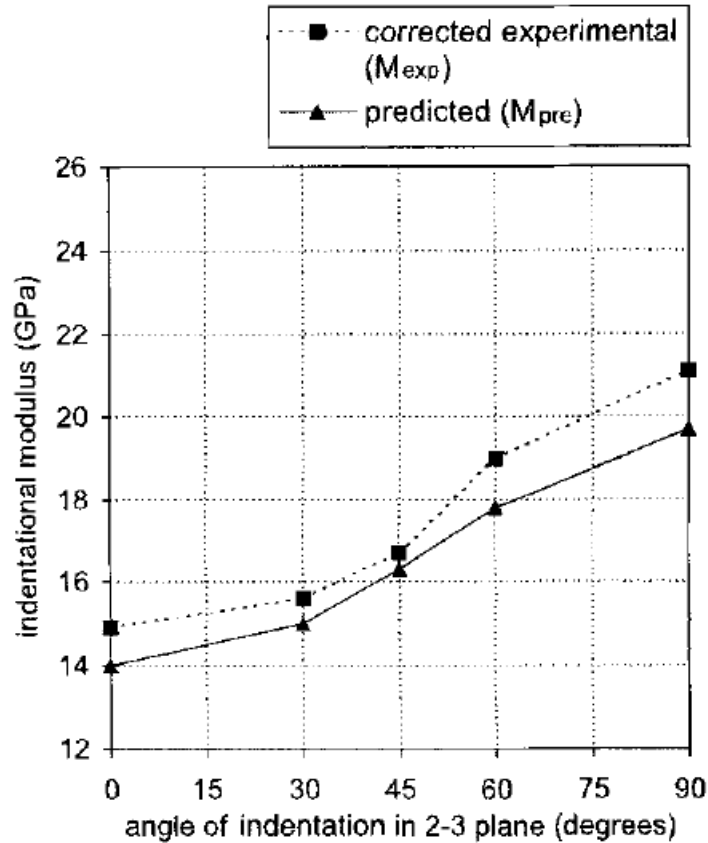
Figure 13: Plot showing the comparison of predicted modulus to the corrected experimental data (corrected data made by assuming 15% increase due to dehydration) [6].

Aging can also affect the characteristics of bone. Researchers have used both animal and human bones to study the effect of the aging on the mechanical properties of the bone. Milovanovic et al. collected eight female femoral trabecular bones (five young adults and three elderly) and embedded the specimens in the epoxy resin. The samples were then prepared by polished using up to 4000 grit papers followed by drying under room temperature. They found the variation of mean modulus and hardness between the elderly (E: 1.28 ± 0.16, H: 0.92 ± 0.12 GPa) and young bones (E: 1.97 ± 0.52, H: 0.59 ± 0.15 GPa). The study suggested that the higher moduli found in elderly bones indicated the lower loading energy that those bones could bear with [16].

17

Gourion-Arsiquaud et al. used the femoral cortical bone from different age baboons to examine the animal age and tissue age effects on the mineral and matrix properties in the bone. The osteon is a tissue that keeps remodeling, thus the structure near the center of the osteon is considered "younger", whereas with increasing distance from the center to the periphery of the osteon, the structure is considered "older". The bone samples were dehydrated in a series of alcohol mixtures and embedded into polymethylmethacrylate. The samples were then polished anhydrously to achieve a root mean square roughness less than 15 nm over a 5 μm x 5 μm area. The Berkovich tip was advanced to 700 μN with 50 μN/s, held for 10 seconds and unloaded to zero with 50 μN/s. They found that mineral-to-matrix ratio increased with increasing distance from the center of the osteon, i.e. higher mineral-to-matrix ratio in older tissue (Figure 14). The modulus significantly increased with the increasing tissue age (Figure 15). Also, the mineral-to-matrix ratio was correlated to the animal age (Figure 16) [10].
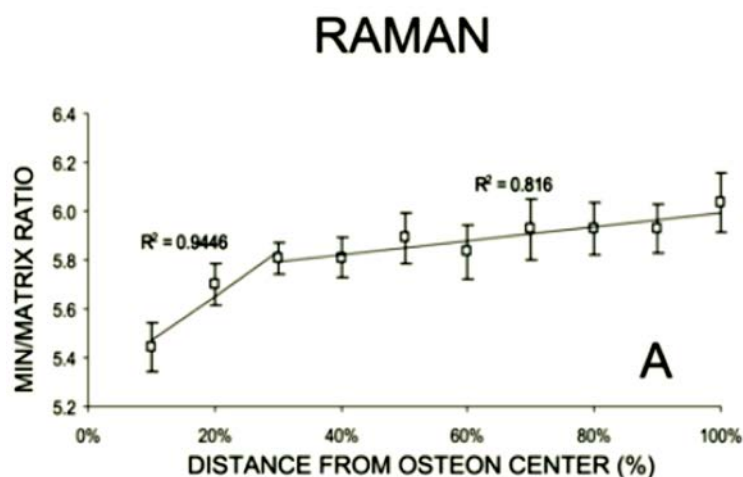
Figure 14: The mineral-to-matrix ratio increasing from the center to the periphery of the osteon [10].
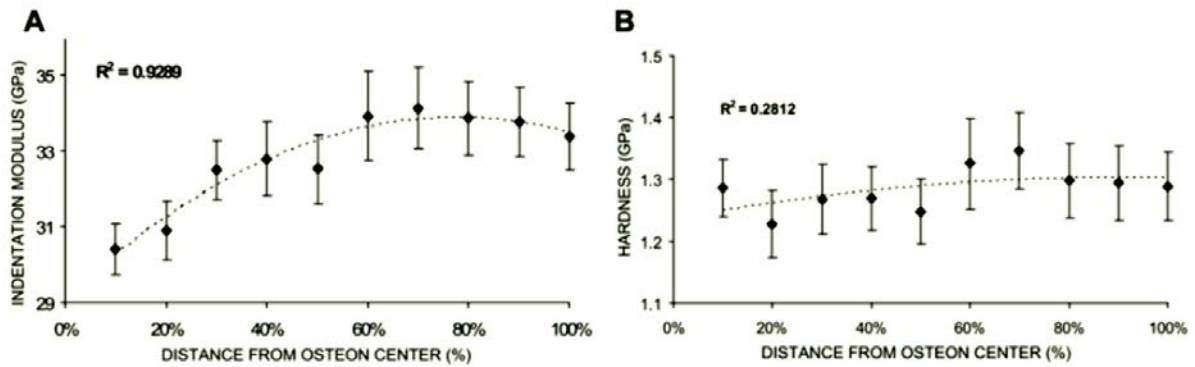
Figure 15: Modulus and hardness increasing from the center to the periphery of the osteon
(A and B) [10].

TABLE 2. FTIRI Properties Correlated With Tissue Age for the Nine Age Groups

Age group (yr)	Min/matrix ratio		CO₃/PO₄ ratio		1030/1020 ratio		1660/1690 ratio	
	Slope	r^2	Slope	r^2	Slope	r^2	Slope	r^2
0	0.61	0.90*	−0.01	0.93†	0.16	0.93†	1.71	0.96†
1	0.68	0.93*	−0.006	0.99†	0.16	0.96*	1.32	0.93†
2.5	0.97	0.91*	−0.006	0.94†	0.16	0.95†	0.84	0.97†
6	0.74	0.99*	−0.007	0.93†	0.23	0.97*	1.71	0.96†
9	0.63	0.96*	−0.007	0.92†	0.19	0.93†	0.97	0.95†
13.5	0.89	0.98*	−0.005	0.96†	0.16	0.94†	0.89	0.96†
18.5	0.91	0.96*	−0.006	0.98†	0.22	0.95†	0.99	0.95†
27	0.77	0.99*	−0.004	0.96†	0.14	0.93†	0.89	0.94†
31	0.92	0.94*	−0.007	0.98†	0.22	0.95†	1.32	0.93†

Slope and correlation reported as the square of the Pearson's correlation coefficient (r^2) for each analyzed IR parameter plotted as a function of the anatomical location inside the osteons calculated for each baboon age groups shown in Figs. 2B, 3B, 4B, and 4D. Each age group consisted of three animals.
* $p < 0.001$.
† $p < 0.01$.

Figure 16: Data from Fourier transform infrared imaging analyzed by regression analysis.
The mineral-to-matrix ratio correlated to the animal age [10].

Burket et al. tested the mechanical properties and the composition of the osteon with aging. Femoral bones from female baboons were used. The samples were fixed in polymethlymethacrylate and polished to achieve a surface roughness less than 15 nm. The indenter was loaded to 700 µN, held for ten seconds and unloaded to zero with a 14 seconds loading and unloading time, generated about a 150 nm indent depth. The results showed

that both mechanical properties increased significantly in the period of maturity with greater than five years being considered mature. The modulus increased 6.6% per year in the young period and 0.2% per year after mature age. The hardness increased 6.8% per year in youth with no significance change after maturity. For the tissue age, the modulus showed no variation but the hardness decreased in mature animals by a total 9-18% across the osteon (Figure 17). The mineral-to-matrix ratio increased 12% per year for young baboons but not after maturity; the ratio was not influenced by tissue age (Figure 18). The modulus and harness varied as the matrix-to-mineral ratio changing (variation 78% in modulus and 70% in hardness) [1].
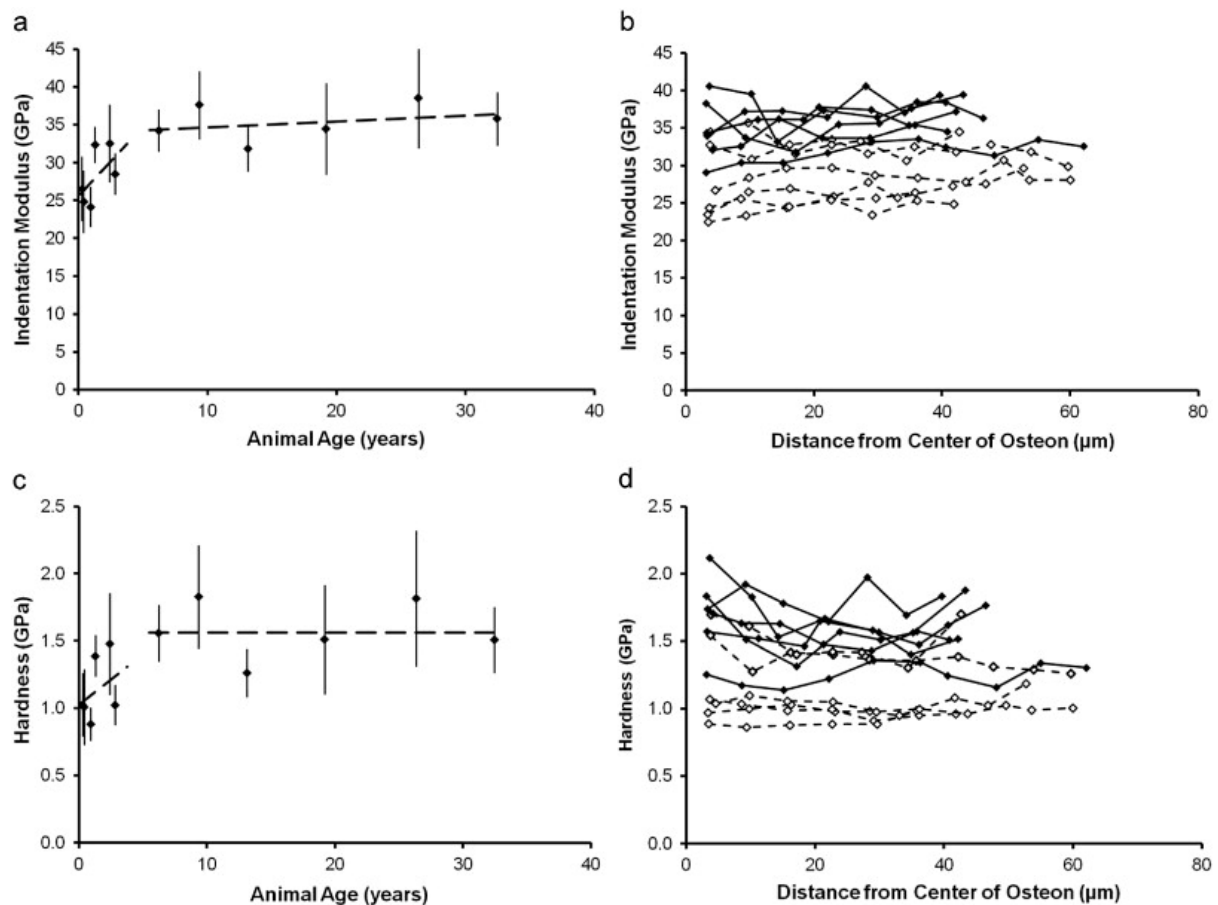
Figure 17: (a) Modulus and (b) hardness increasing with the animal age. (c) (d) Mechanical properties corresponding to tissue age [1].
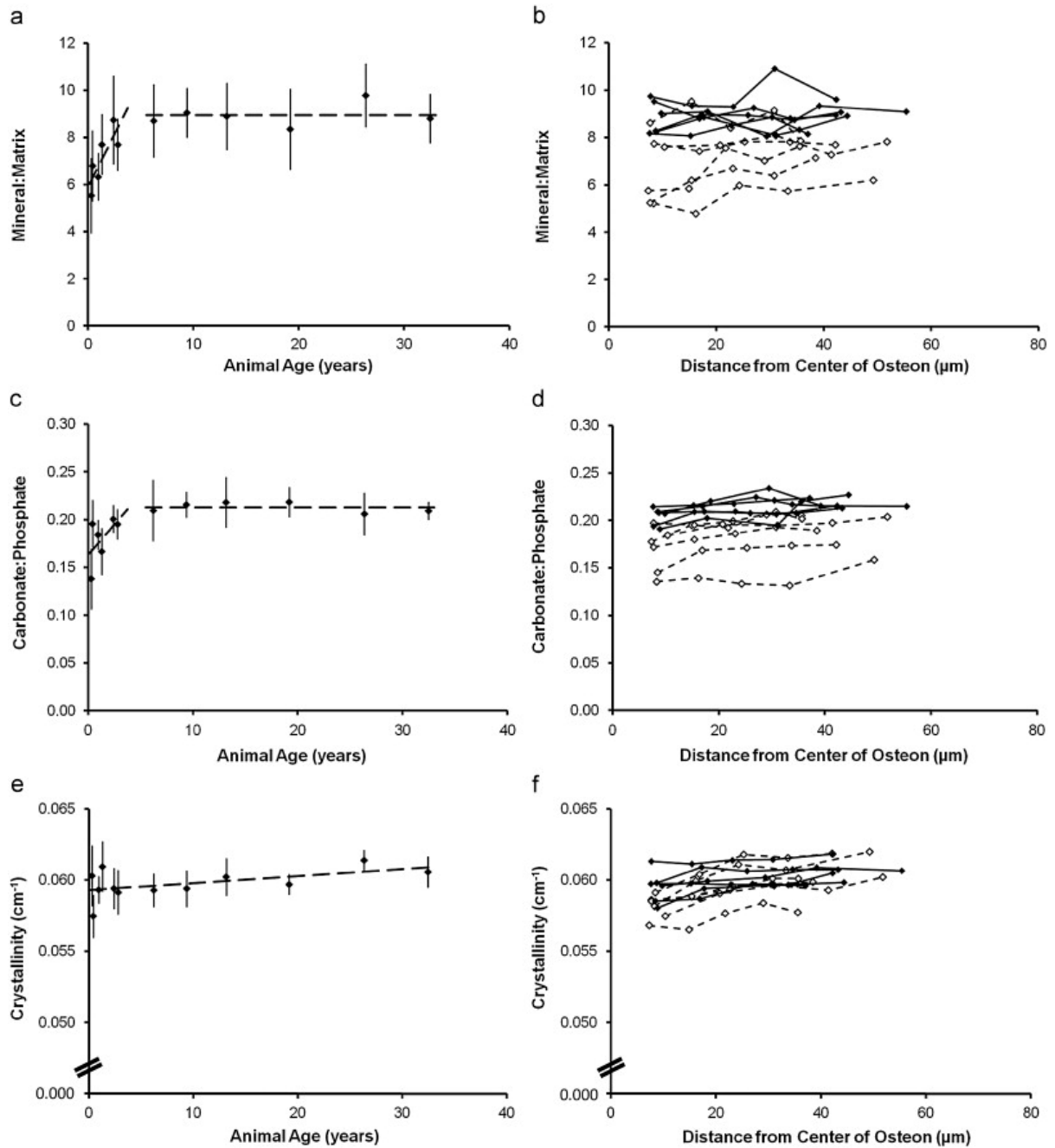
Figure 18: Plots (a) (c) (e) showing relations between the bone composition and the animal age. Plots (b) (d) (f) showing the bone composition and the tissue age (b) (d) (f). Plots (a) (b) showing mineral-to-matrix ratio. (c)(d) Carbonate: phosphate (e) (f) Crystallinity [1].

Feng et al. tested the porcine bone to show the relations of elastic modulus and hardness to four factors: ages, sample positions (laminar, interstitial or osteon), hydration

and testing directions. The bone samples, from 6, 12, and 42 month porcine femurs, were polished using abrasive papers (up to 4000) and aluminum micro-cloth (3 µm, 1 µm, 0.25 µm and 0.05 µm). The loading protocol was a trapezoidal shape loading function consisted of a five seconds loading, five seconds holding and five seconds unloading time with a 2000 µN maximum load. It was found that all four factors have certain degree of influence on the modulus and hardness. With age increasing, both values increased differently depending on the tissue type, i.e. osteon, laminar bone or interstitial bone. Except for interstitial bone, laminar and osteon bone demonstrated higher modulus and hardness in the 42 month sample. The modulus of the laminar bone in the longitudinal direction was higher than that in the transverse direction in the 6 and the 42 month sample. The hardness of the laminar bone was only higher in the longitudinal direction for the 42 month sample (Figure 19). The modulus in osteon was 42% higher in the dehydrated sample than in the hydrated sample (modulus~27 GPa, hardness~0.9 GPa in the longitudinal direction in dry sample). On the other hand, a 26% increase of modulus in interstitial bone was found in dry sample compared to wet sample (Figure 20) [7]. This study provided a great deal of information of the mechanical properties under several factors.
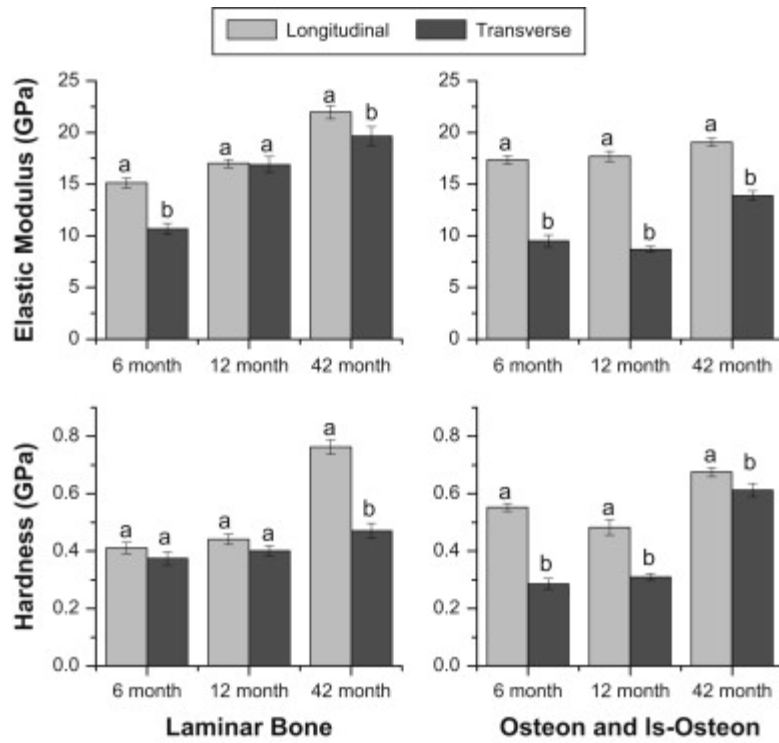
Figure 19: Property comparison for different directions with differing ages [7].
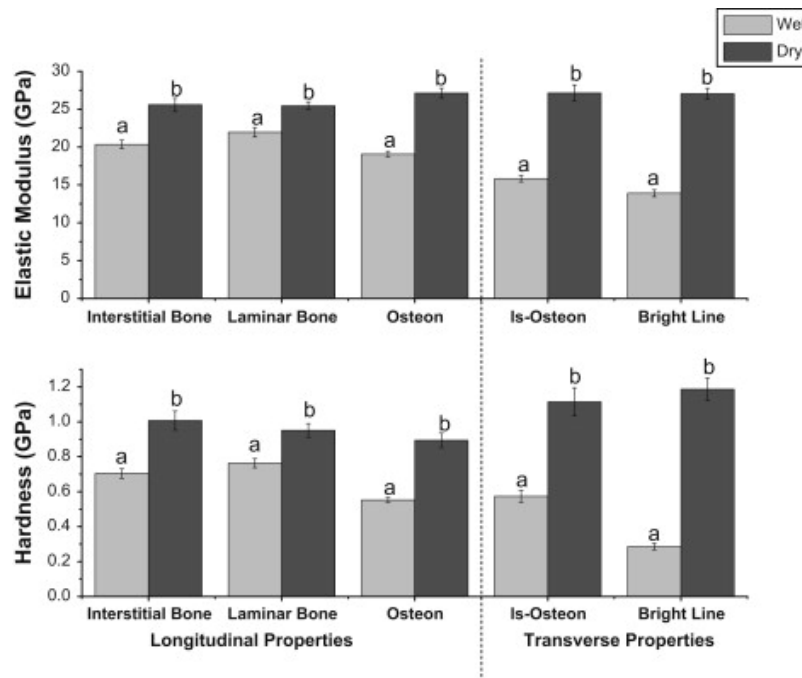
Figure 20: Comparisons for wet and dry samples with different microstructures [7].

2.2 PROBLEM STATEMENT

Among these studies, it is clear that the mechanical properties are correlated to the composition of the bone structure, and are related to the testing condition (dry or wet), testing direction, age, and the location of the bone sample (e.g. thoracic or lumbar spine). To the best of the author's knowledge, there has been no research focused on the variation of the modulus and hardness in the different regions of the cortical bones of the porcine femur and the tibia. Hence, one purpose of this study was to examine the modulus and the hardness variations in the anterior and posterior regions of the bone. Osteon bone was picked as the testing target because it also exists in human body, which may provide some reference for future study on human. Additionally, this study also compared the mechanical properties in the femur and the tibia. The goal was to have a view of how mechanical properties change through the tibia to femur in different directions and regions (anterior and posterior). This study used dry samples since testing wet sample required more complicated testing skills and equipment.

3.0 MATERIALS AND METHOD

3.1 SAMPLE PREPARATION

Two porcine legs were acquired from the local butcher. After stored in the freezer at -20℃, the soft tissue was removed from the bone followed by sawing transversely to obtain three 1.5 cm sections from the mid-section of the tibia and femur. This length was selected for convenience for polishing process. The location and the direction were marked on the sample (Figure 21).

To test a specimen with a surface in the longitudinal direction (x direction, shown in Figure 22), the first sample of bone was used. The second cylinder was cut in sagittal plane (y plane) to obtain a brick shape sample (Figure 23). The last piece was polished directly to obtain a flat frontal plane (z plane) (Figure 24).

Figure 21: Femur (up) and tibia (down) cut from porcine leg with mark of direction.

After the marrow was removed, the bone surface was polished with constant water irrigation with 400, 600, 800 and 1200 silicon carbide grinding papers (Buehler UK Ltd., England) and a polishing machine (Buehler UK LTD., England). Following that, the samples were further polished using 1 µm and 0.05 µm aluminum powders (Struers, Danmark). Each sample was polished carefully to achieve a flat, smooth surface for nanoindentation. The samples were then examined by digital microscopy (VHX-600 Keyence, Japan) and photographed to show clear views of the marked bone structures, i.e. osteon (Figure 25). The ink mark was used for locating the osteon again when doing nanoindentation. The samples were dried for 24 hours at room temperature prior to testing [7] and finally mounted on the thin steel strips (Astra Superior Platinum, Russia) using super glue (Loctite, Germany) half hour before indented.
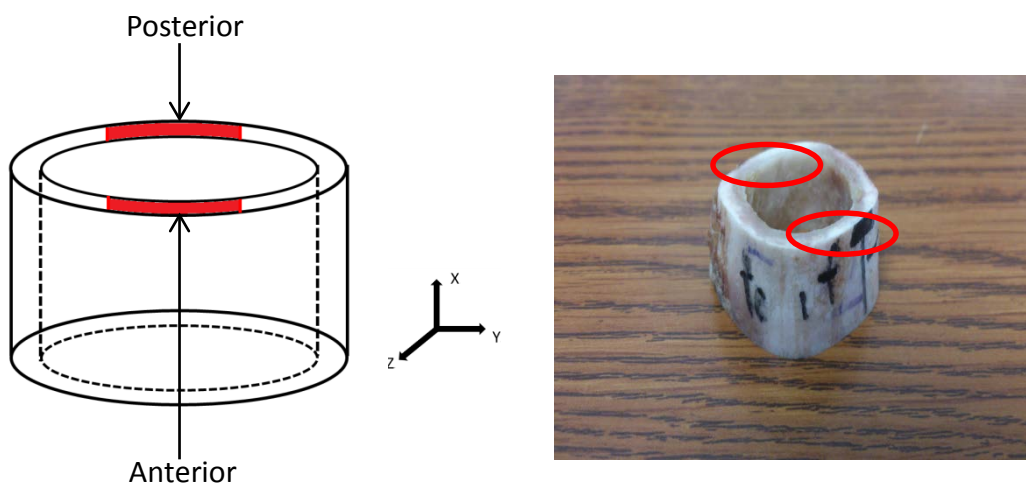
Figure 22: Scheme showing red Indicated area representing two locations of interest in longitudinal direction (x direction).

Posterior
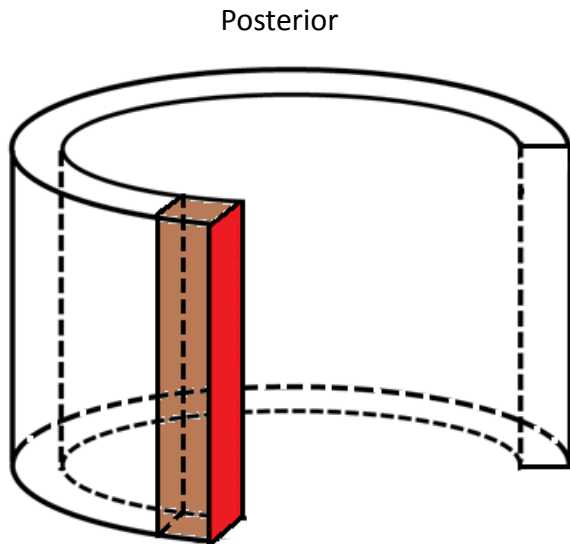
Figure 23: A brick shape sample cut off from the second part of the bone sample. Red painted region indicating the plane of interest (y direction).

Posterior
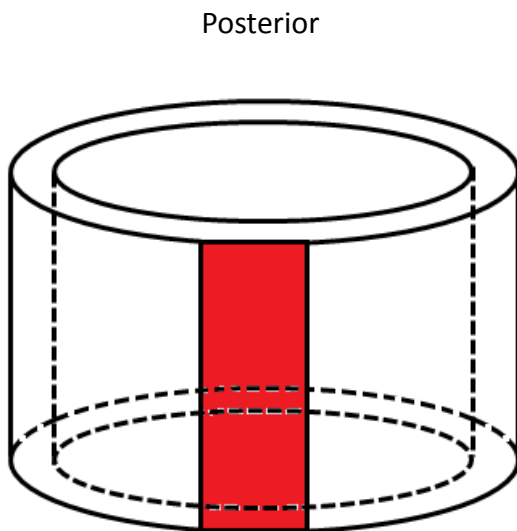
Figure 24: The indented region indicated in red in the z direction on the sample.
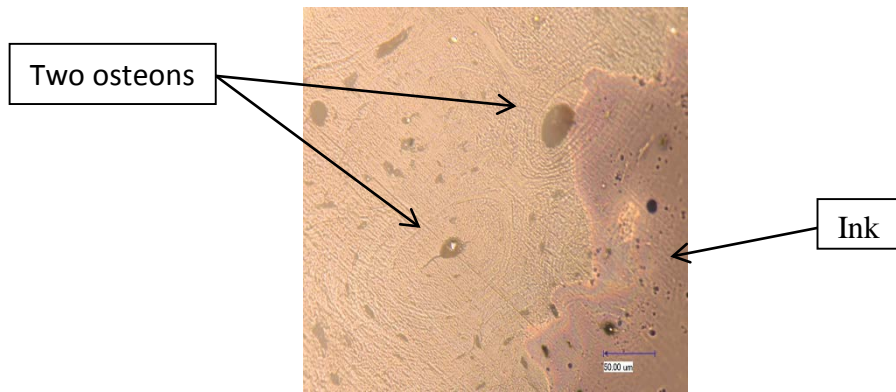
Figure 25: Photograph from the digital microscopy. Two osteonal structures in the middle

and the ink mark at the right side of the picture to record the position of interest.

3.2 NANOINDENTATION

In this study, for convenience, the x, y and z directions were used to represent the indent direction. The femur and the tibia are two bones, and four regions of each bone were to be examined, i.e. the x direction of the anterior region, the x direction of the posterior region (Figure 22), the y direction of the anterior region(Figure 23) and the z direction of the anterior region (Figure 24). At least three osteons (three areas) were picked in each region, and 5 - 7 indents were carried out in each area to average the measured values.

The nanoindentation tester used in this study (TI900 Hysitron Triboindenter, Hysitron, USA) was equipped with a three side pyramidal Berkovich tip (Figure 3). The tip was made of single crystal diamond with an angle of 142.3° and radius of the curvature of 150 nm. Prior to testing, the sample was imaged by scanning probe microscopy (SPM) to locate the position of interest, and quantify the roughness of the surface with a 40 µm scan size (Figure 26). After polished, the surface achieved an average roughness ranging from 30 - 80 µm over a 40 µm x 40 µm area. After checking the surface condition for any damage, a smaller scan size, 20-40 µm, depending on the size of the structure, was then used to further position the area to be indented.
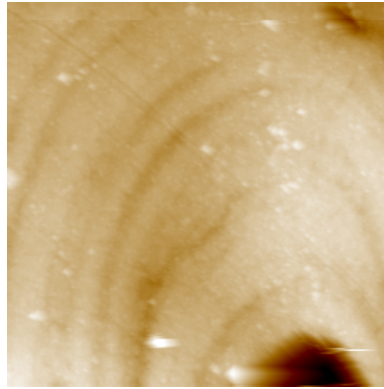
Figure 26: The scanning probe microscopy image with a 40 µm x 40 µm dimension of an

osteon structure in the porcine femur.

The load function used for indentation was composed of a 5s loading phase followed by a 5s holding and 5s unloading time (Figure 27) [7]. The 5s holding time was used to avoid creep behavior and the "nose" shape (Figure 28), which can affect the analysis of the unloading segment and thus result in inaccuracy. Specifically, the calculated reduced modulus (E_r) accounts for the stiffness (S), calculated by fitting the slope of the load-displacement curve. The "nose" shape curve generated from creep behavior will lead to a higher or even negative S, causing the error of the reduce modulus. While other studies selected different holding times [29-31], Wu et al. suggested that the results are valid if the load function is consistent through the experiment [23]. However, if the dwell time is set too long, the drift factor resulting from the vibration of the system or external interference would also cause inaccuracy.
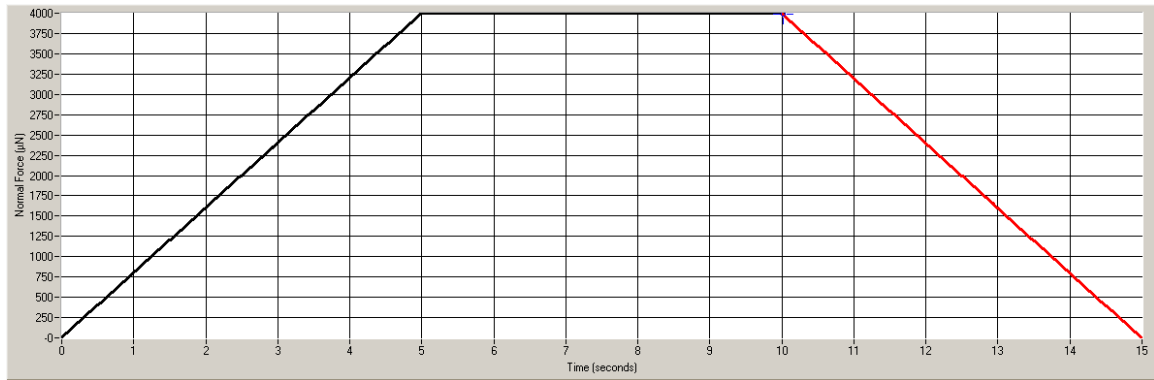
Figure 27: A 5-5-5 trapezoidal load function with maximum 4000 μN.

(a)   (b)
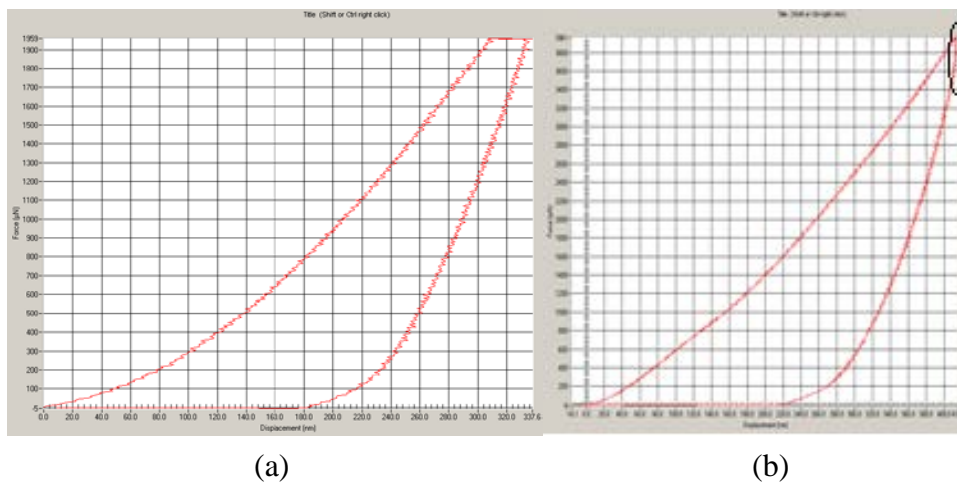
Figure 28: (a) Normal force-displacement curve using a 4000 μN, 5s loading, 5s holding and

5s unloading time. (b) Nose shape generated from creep without holding time.

In the previous study, Feng et al. used 2000 μN as the peak load [7]. However, the

samples were all submerged in the fluid thus softer and required a smaller force to achieve

the desired indent depth. The peak force in this study, since the samples were all

dehydrated, was selected to be 4000 μN to give approximately a 400-600 nm indentation

depth depending on the indent position. The max load can assure that the indent depth is at

least three times higher than the surface roughness, thus the roughness effect could be

eliminated [30] and massive damage in the osteon structure could be prevented [32].

31

The spacing between each indent was selected to be five times of the diameter of the indent size based on the ISO standard for indentation (ISO/FDIS 14577-1). While some studies used 3-5 times of the indent width as a standard (Feng et al. 2012), this study followed the five times indent width recommendation. This spacing is for avoiding overlap of the residual plastic deformation which can affect the results. After the indentation, the in-situ imaging was again performed to check the position of the indent (Figure 29).
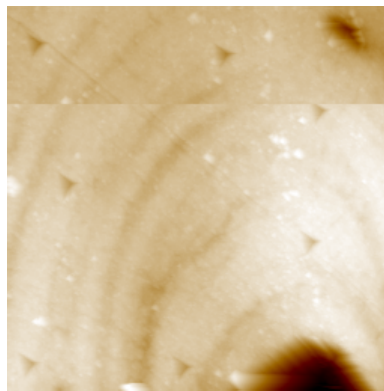
Figure 29: The surface image after seven indents.

3.3 STATISTICAL ANALYSIS

This study aims to compare the mechanical property variations throughout the tibia and the femur. Two porcine sets of bones were used in this study: the femur and the tibia; each bone has three test directions. For the x direction, it was further divided into the anterior and posterior region. Each region, was tested at least three small areas; finally, five to seven indents were conducted in each area. The purpose of choosing three small areas and five indents were to be able to average the obtained values and avoid the extreme values. Since indents were in three small areas, it is reasonable to see if there is any difference between areas. Table 1 shows the number of areas and the total number of indents for each region

and direction, e.g. there are four picked areas and a total 28 indents in the anterior region of the femur of pig1.

The one-way ANOVA was used to compare the difference between the anterior region and posterior region. The Tukey test was used to analyze the data from each area within the same region, and the data from different directions in the same bone. $P<0.05$ represents significant difference.

Note that the one-way ANOVA can only tell that there is a difference among all sets of data but is not able to specify which set, thus it was only used in anterior-to-posterior case. For the comparisons more than two sets, the Tukey test was used and is able to do pair-to-pair comparisons.

Considering the individual effect, that variations may exist among the two samples, the linear mixed model was used. The linear model is to model, the mechanical property as a function of testing direction with a random error term, and the testing direction is a fixed effect. In this study, two samples were used, thus the measured data may be dependent. In this case, statisticians add random effects term to represent the individual difference. So the "fixed effect" and here "random effect" makes up the "mixed model". The linear mixed model is able to tell if a factor of interest plays a role in affecting the mechanical property. For example, the bone (femur or tibia) is a factor of interest, and the model can indicate that whether or not the mechanical property is significantly different in the femur and tibia. Data from the two samples was combined and analyzed by linear mixed model for comparison between each region.

R (64bit, 3.0.3) is a free statistical analysis software and was used in this study. The one-way ANOVA, Tukey test and linear mixed model were all coded in the program to do the analysis. Details for the code can be found in the Appendix D.

Table 1: Total number of data points from each sample.

		Axial Anterior (X)		Axial Posterior (X)		Sagittal (Y)		Frontal (Z)	
		Area	Total indents	Area	Total indents	Area	Total indents	Area	Total indents
Pig 1	Femur	4	28	4	28	4	28	4	28
	Tibia	7	35	5	25	7	35	4	20
Pig 2	Femur	3	18	3	17	4	20	3	20
	Tibia	3	15	5	25	3	16	3	18

4.0 RESULTS

In this section results are broken down as follows. Section 4.1 compares the reduced modulus and hardness between different areas in the same region. Section 4.2 shows the differences in material properties between anterior and posterior regions. Section 4.3 will focus on the mechanical properties comparison between x, y and z directions. Last but not least, Section 4.4 gives the results of the femur and the tibia.

Results of the measured data and statistical analysis will be presented. For convenience, from now on all locations are named by the order of sample number-bone-direction-region-area. For example, 1FemurXA1 represents the pig1, femoral bone, x direction, anterior region and area1.

4.1 COMPARISON OF PROPERTIES BETWEEN DIFFERENT AREAS

Figure 30 and Figure 31 are examples showing the measured hardness from different areas in the same region. In Figure 30, the hardness measured in the four areas have no significant difference between each other, hence the same letter "a", was marked on the top of the bars. On the other hand different letters, "a", "b" and "c", were used in Figure 31 to indicate that statistical differences exist between each set of data.

All of data are given in Appendix A. Note that letters are used only in the examples, since that p values are given in Appendix B.

Figure 32 is an example for the p values between each areas calculated by the Tukey test. The horizontal axis labels gives the area number in the specified region, e.g. 1FemurXA 1-2 represents area1 compared to area2 in 1FemurXA. The line in the chart indicates p=0.05, hence any bars underneath the line have a significance result found in the comparison. Appendix B also gives the bar charts of p values for area to area comparisons.
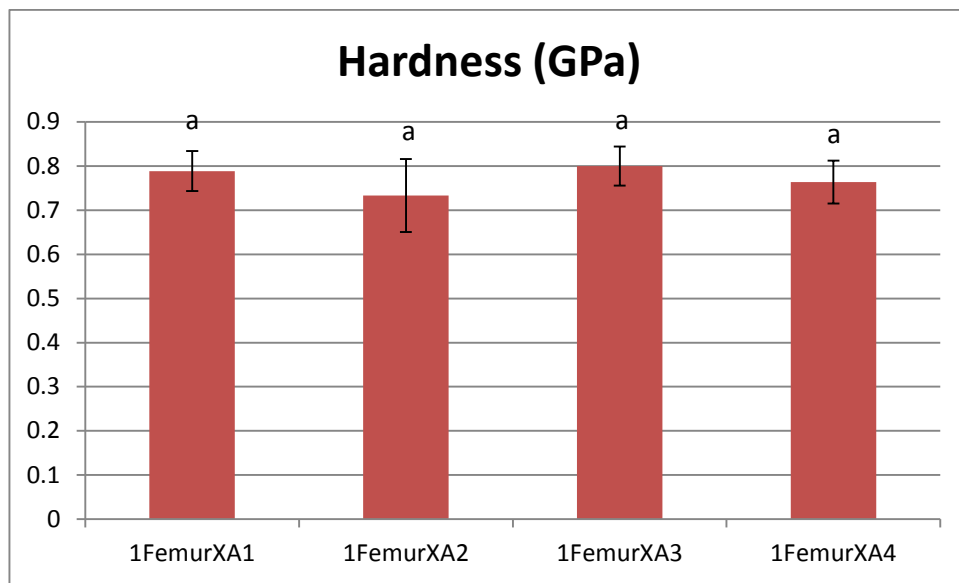
Figure 30: Hardness measured from area1 through area4 in 1FemurXA. Same letter used to indicate no significant differences found between each other.
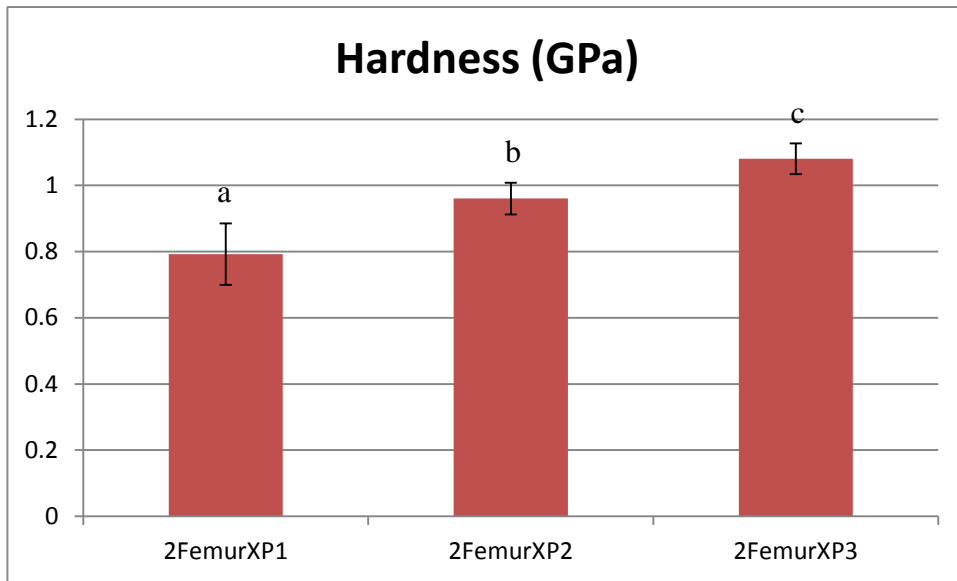
Figure 31: Hardness measurements from area1 through area3 in 2FemurXP. Three letters used to indicate significant differences found between each area.
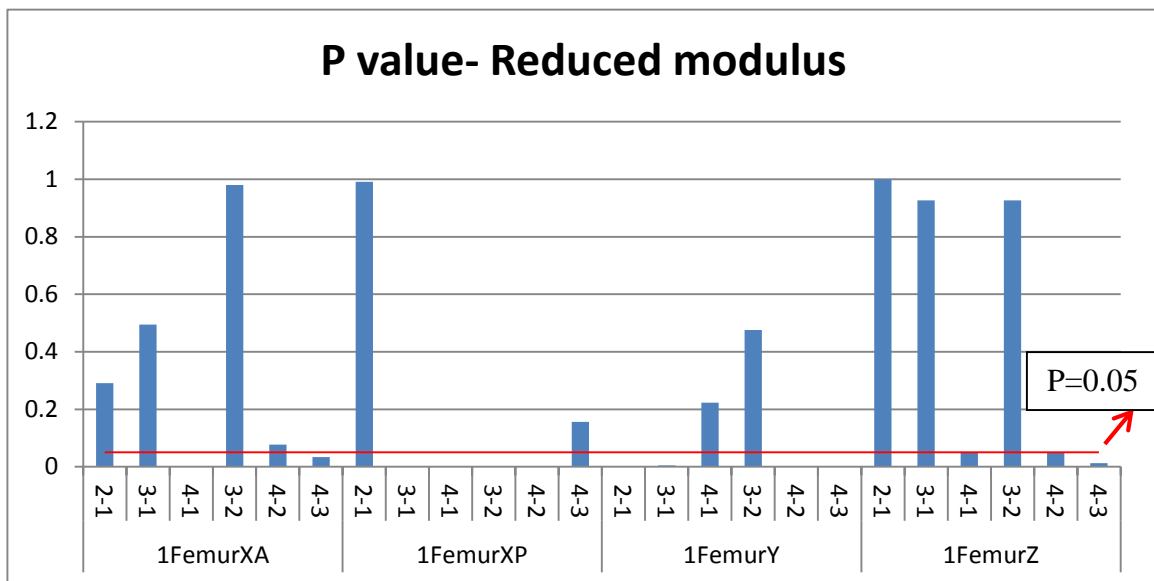
Figure 32: P values of the area to area comparisons of the reduced modulus in 1Femur by the Tukey test. Line indicating p=0.05. Bars under the line indicating that a significant difference is found in this compared set of data.

4.2 COMPARISON OF ANTERIOR AND POSTERIOR PROPERTIES

After the area to area comparison, measured properties from all areas in the same region were averaged for further comparisons. Figure 33 shows the average and the standard deviation of the mechanical properties for anterior and posterior regions of both pig1 and pig2. Table 2 gives the p values of each anterior-to-posterior set by a one-way ANOVA analysis with p value less than 0.05 being considered significantly different. Note that p value less than 0.0001 will be listed as zero.
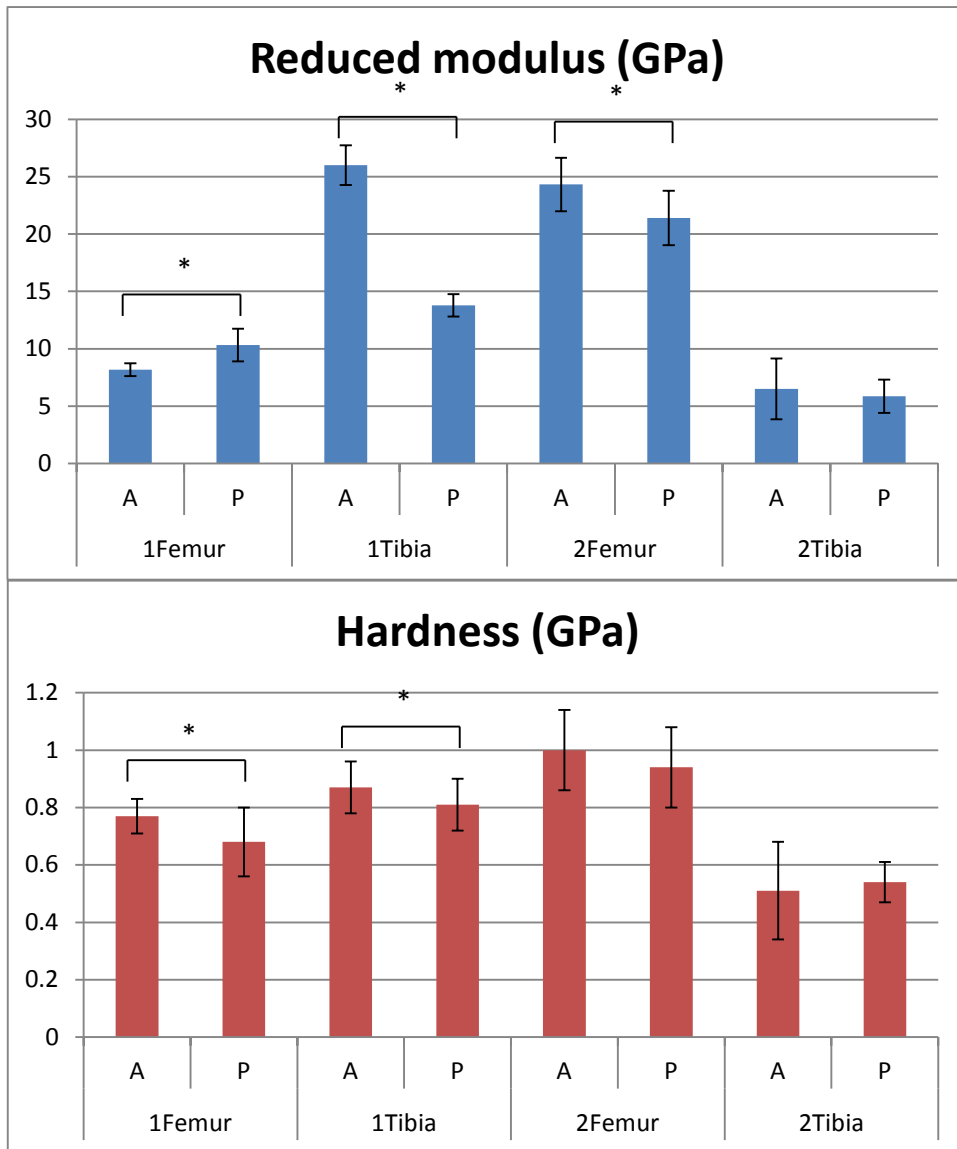
Figure 33: Reduced modulus and hardness in the anterior and posterior regions for the femurs and tibiae in x direction from pig1 and pig2 (* p<0.05).

Table 2: P values from a one-way ANOVA of the mechanical properties between anterior and posterior regions in the femur and tibia of pig1 and pig2 (value given as 0 if p<0.001).

Pig Number	Regions	P value	
		Reduced modulus	Hardness
1	Femur A to P	0	0.0011
1	Tibia A to P	0	0.008
2	Femur A to P	0.0008	0.194
2	Tibia A to P	0.338	0.454

4.3 COMPARISON OF PROPERTIES IN DIFFERENT DIRECTIONS

Figure 34 gives the mechanical properties of the porcine bone as measured in different directions. Significant differences between each direction were marked by different letters. Table 3 is the comparison using the Tukey test between properties in the x, y and z directions. Note that this is only for comparisons between same bone (femur or tibia) from the same animal.
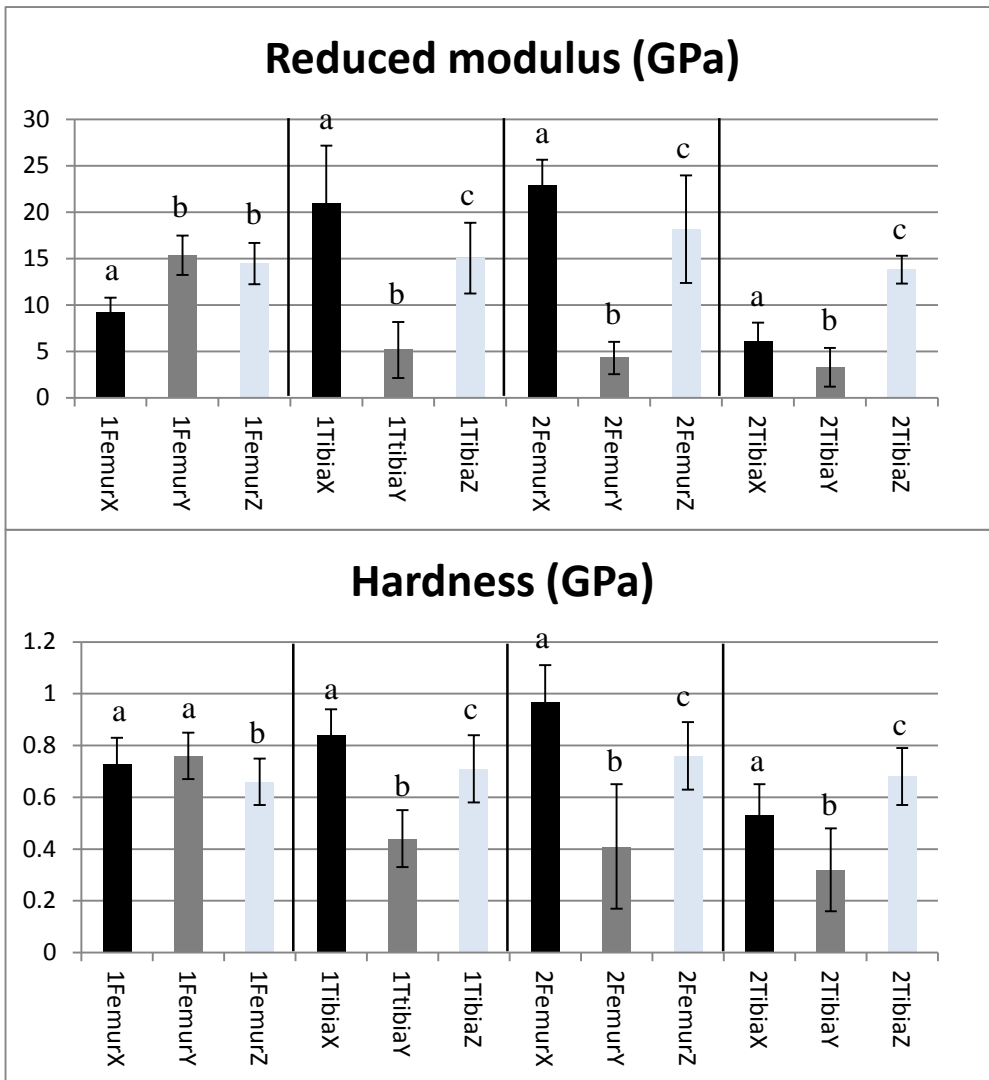
Figure 34: Properties for the different directions in the femurs and tibiae in both animals.

Different letters indicating significant difference (p < 0.05) between data in each direction.

Table 3: P values for the property comparison in the different directions by the Tukey test.

Pig	Part	Direction	P value-Er	P value-H
1	Femur	x to y	0	0.4201
		x to z	0	0.0097
		z to y	0.1741	0.0011
	Tibia	x to y	0	0
		x to z	0.0001	0
		z to y	0	0
2	Femur	x to y	0	0
		x to z	0.0001	0.0002
		z to y	0	0
	Tibia	x to y	0	0
		x to z	0	0.0015
		z to y	0	0

4.4 COMPARISON OF FEMORAL AND TIBIAL PROPERTIES

In this section, the mechanical properties of both samples were combined and compared between different bones in the same region, or the same bone in different regions. In Figure 35, for example, 1FemurXA, 2FemurXA were combined and compared with 1TibiaXA putting with 2TibiaXA. Note that the diagram only shows the data sets in x direction; data in y and z direction were also included in the analysis.

The linear mixed model is used to analyze the measured data and is able to tell if the factor of interest plays a role on the change of mechanical property. The model contains the random effect term to describe the individual difference. The raw data from the linear

mixed model analysis are shown in Appendix C. P values were calculated and are shown in Table 4.

The raw data was converted back to the mean values of hardness and reduce modulus for each region for both pigs by equation (4),

$$y = A + B_{Tibia} \times X_{Tibia} + B_{DY} \times X_{DY} + B_{DXA} \times X_{DXA} + B_{DXP} \times X_{DXP} \text{ (4)}$$

where y is the estimated mean value of the mechanical property; A is the intercept; B_{Tibia}, B_{DY}, B_{DXA}, B_{DXP} are calculated constants given in the table in Appendix C. X_{Tibia}, X_{DY}, X_{DXA} and X_{DXP} are variables that are either 0 or 1 to representing the region number, direction and bone.

For example, to compute the reduced modulus of FemurXA, according to Appendix C, A, B_{Tibia}, B_{DY}, B_{DXA}, B_{DXP} are 8.40891, -1.7843, 7.55051, 9.76954 and 4.55402 respectively. X_{Tibia}, X_{DY}, X_{DXA} and X_{DXP} are set 0, 0, 1, 0 respectively. Note that 0 means the corresponding term is knocked out and 1 means the corresponding term remains. Since femur is the bone of interest, X_{Tibia} has to be 0. If tibia is to be considered, then X_{Tibia} has to be 1.

Another example is that, to compute the hardness of TibiaZ, X_{Tibia}, X_{DY}, X_{DXA} and X_{DXP} are 1, 0, 0, 0 respectively. A, B_{Tibia}, B_{DY}, B_{DXA}, B_{DXP} are 0.55574, -0.1129, 0.1844, 0.30251 and 0.22418 respectively, according to Appendix C.

The estimated mean values of mechanical properties from the combined samples for each region are shown in the Figure 36. Different letters were used to indicate significant differences. Figure 37 shows the comparisons of the mechanical properties in the femur and the tibia.
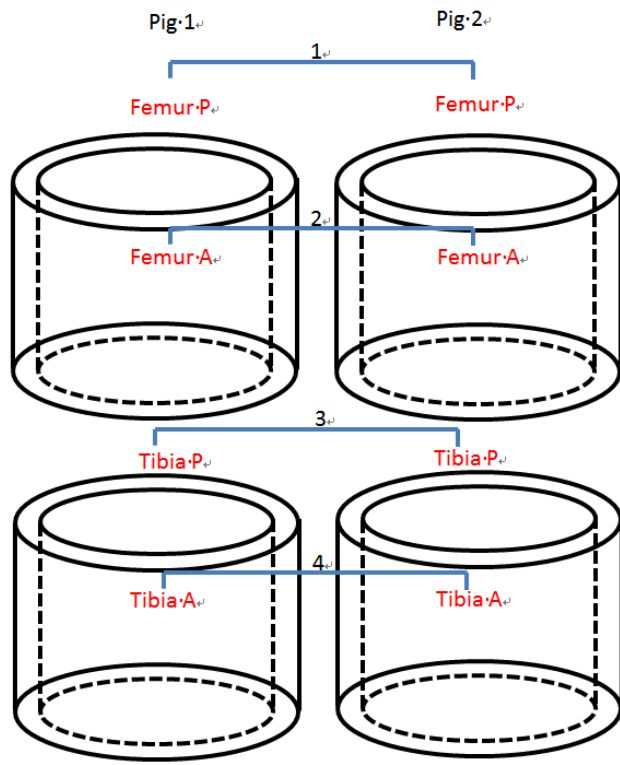
Figure 35: Diagram indicating the adding different sets of data from pig 1 and pig 2.

Comparison made between each number.

Table 4: A summary of p values for comparisons for all regions, directions and bones.

	P value	
Compared sets	Er	H
Femur to Tibia	0.0073	0
Y to Z	0	0
Y to XA	0	0
Y to XP	0	0
Z to XA	0.021	0
Z to XP	0.002	0.1235
XA to XP	0	0.0016
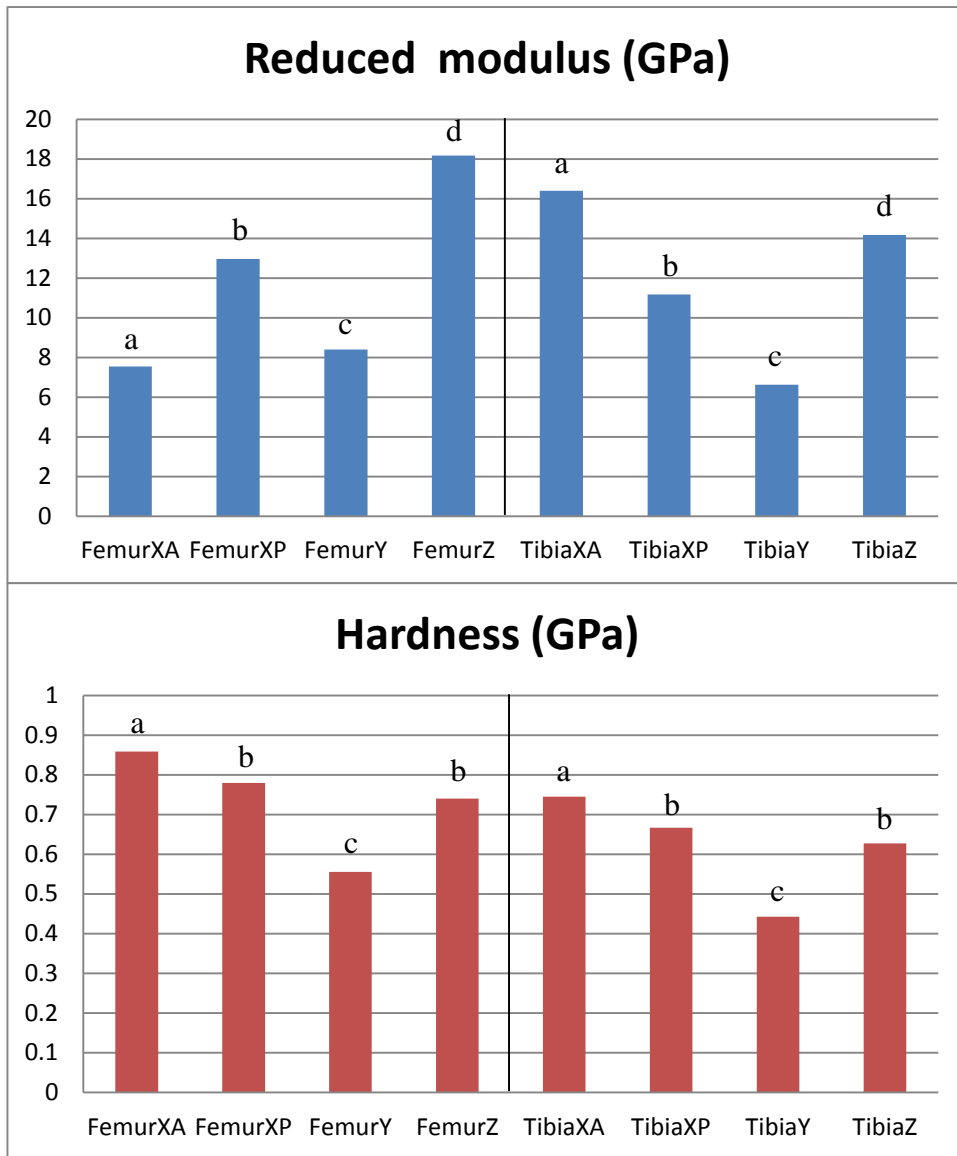
Figure 36: The mean values of each region for pig1 and pig2 calculated by equation (4).
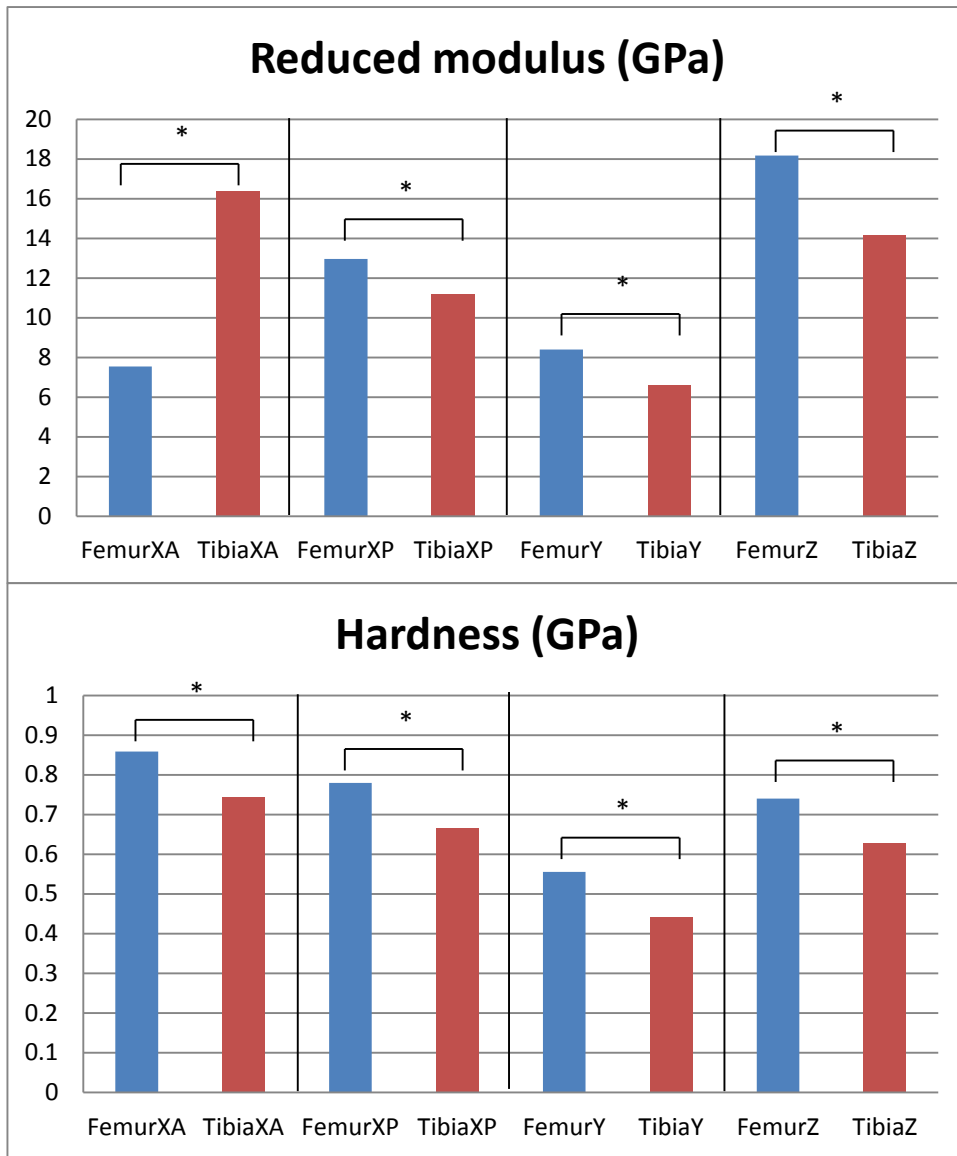
Figure 37: Comparisons for the properties between the femur and the tibia. In general, the mechanical properties in the femur are higher than those corresponding to the same region in the tibia.

5.0 DISCUSSION

Bone is the structure with hierarchy and anisotropy [6, 20]. The mechanical properties vary with many factors including age, gender, direction, location, etc. [1, 7, 9, 16]. To understand the bone structure, the reduced modulus and hardness were measured by nanoindentation to investigate the variations in the porcine tibia and femur.

The modulus considered in this paper is reduced modulus. It should be noted that reduced modulus obtained from the test accounts for the sample elastic modulus, Poisson's ratio and the indenter's elastic modulus and Poisson's ratio (1). The elastic modulus and Poisson's ratio for a diamond tip are fixed, and the Poisson's ratio for the bone is assumed to be 0.3 [7, 9, 21]. Under this assumption, the elastic modulus is about 1.1 times greater than the reduced modulus.

In the following sections, Section 5.1 gives a discussion about the mechanical properties comparison between different areas in the same region. Section 5.2 discusses the mechanical property variation in the anterior and posterior region and compares the result to other studies. Following that, Section 5.3 gives a discussion for the mechanical properties measured in different directions. Section 5.4 gives some discussions about the result from the linear mixed model and potential factors affecting the material properties. Last but not least, Section 5.5 points out the limitation and the prospect of this study.

For the directions mentioned in the following paragraphs, as a reminder, the x testing direction (y-z plane) is the axial direction; the y direction (x-z plane) corresponds to the sagittal plane and the z direction (x-y plane) is the frontal plane.

5.1 COMPARISON OF PROPERTIES BETWEEN DIFFERENT AREAS

Mean values with the standard deviation at each area of all samples are given in Appendix A and the details of the p values are in Appendix B.

The results show, from Table 5, that some regions have large variation. Regions, in which half of areas showed significant differences, were considered having large variations and are marked by X in the Table 5. Taking Figure 31 as an example, the hardness in the 2FemurXP are statistically different, thus the row "2FemurXP" corresponding to the column "hardness" was marked by X.

No significant differences in reduced modulus were found in 12 out of 16 regions; hardness was the same in 14 out of 16 regions (Table 5). Regions with variation are all in the pig2 (Table 5). This indicates that pig1 has uniform properties in all regions, i.e. mechanical properties measured in different areas of a region have no significant differences. In contrast, variations in the mechanical properties in different areas of a region were found in many regions of pig2. This indicates that individual differences may have an effect on the mechanical property variation in the area.

5.2 COMPARISON OF ANTERIOR AND POSTERIOR PROPERTIES

In pig1, the reduced modulus and hardness in the anterior region vary from those in the posterior region in both femur and tibia; while in pig2, this trend only observed for the reduced modulus in the femur. This result shows that locations (anterior or posterior) may play a role in the mechanical properties. This result is somewhat consistent with previous studies done by Riggs et al. [48], Bonney et al. [43] and Rho et al. [37]. Riggs et al. found significant differences of mechanical properties between cranial and caudal cortices of

49

equine radii. For example, tensile elastic modulus was 22 GPa for cranial and 15 GPa for caudal cortex (p<0.001).

Bonney et al. found there is regional effect in the porcine femur. For instance, using bending test, they found the posterior quadrant was stronger than the lateral quadrant (241.4±10.43 MPa to 162.3 ± 17.96 MPa in bending strength).

In addition, using the same horse specimen, Rho et al. also showed that for testing in the x direction, the osteons in the anterior region were stiffer than those in the posterior region. However, the result is in contrast to the study done by Giambini et al. using human vertebrae [9], in which no difference was found within each section of the vertebrae, e.g. properties in T7 are the same in both anterior and posterior parts.

To further explain why the anterior portion shows greater mechanical properties, it is known that porcine femur has a certain degree of anterior curvature [51], thus it is possible that the anterior region bears a higher load and become stiffer and stronger.

5.3 COMPARISON OF PROPERTIES IN DIFFERENT DIRECTIONS

For directions shown in Section 4.3, except for the 1Femur, it shows a very similar trend of mechanical properties. For reduced modulus, the measured value in the x direction are the highest (except for the tibia in pig2), followed by those in the z direction, and the reduced modulus in the y direction are the lowest. For hardness, except for the tibia in pig2, it also shows x direction is the highest, followed by z direction, and then y direction. This result suggests the anisotropy of the bone structure and is consistent with the previous study [7, 35-37], in which they all showed the anisotropy mechanical properties of the bones, including porcine, human and equine bones.

The mean values of the reduced modulus in the femur in the x direction obtained here are 9.25 ± 1.53 GPa and 22.90 ± 2.74 GPa for pig1 and pig2, respectively. Multiplying the reduced modulus by 1.1 to obtain an approximate value of elastic modulus gives 10.18 and 25.19 GPa. The value 25.19 GPa is similar to that found by Feng et al. [7] (~27 GPa). The hardness in the x direction is 0.73 ± 0.1 GPa and 0.97 ± 0.14 GPa for pig1 and pig2, respectively. Again, the value measured in pig2 is quite consistent with that in the Feng et al. study (~0.9 GPa). Appendix E gives a comprehensive comparison of the mechanical properties bone measured by nanoindentation in this study and in previous studies.

For the differing results found in the two animals, there may be a difference in gender or other factor that is not known or just due to individual variation. The other possibility for discrepancy of two pigs is the tissue degradation. The specimens were stored in the freezer at -20℃ for a unknown time and have been taken out for other use and then refrozen again, thus it may cause tissue deteriorate. However, previous studies do not have a uniform result on freezing effect [43-47], thus this is still an unknown factor.

Due to time limitation, the experiment was restrained down to only two porcine legs, hence it can only prove that variations do exist in these regions. It may be able to discover the certain pattern of variations in the bone if more samples were tested.

5.4 COMPARISON OF FEMORAL AND TIBIAL PROPERTIES

Comparing the differences between bones and directions, shows the trend that for reduced modulus in the femur, z direction is the highest, and then anterior region in x direction, followed by y direction. For reduced modulus in the tibia, it shows anterior region in x direction is the highest, followed by z direction, and then y direction. Also for hardness both in the femur and tibia, it shows that anterior region in x direction has the greatest hardness,

and z direction is the second high, followed by y direction. This indicates that the orthogonal mechanical property may exist in the porcine bone, and the result agrees with the previous studies [6, 35-37]. The porcine bone structure may be a laminated composite with most fiber orientated toward x direction, some fiber oriented z direction, and laminated direction being y direction. This kind of structure can explain the variation of the mechanical properties in different directions.

This concept matches the plywood-like structure found in the bone by Weiner et al. [38-40]. Figure 38 shows the SEM images and schematic illustrations of several types of bone structures [40]. The third type of bone structure shown in Figure 38 has two fiber orientations and a layer direction, which can explain the mechanical properties are higher for x and z directions while lower in y direction.

It is also observed that except for anterior region in the x direction in the femur, mechanical properties of the femur are always greater than those of the tibia corresponding to the same region. This may be again related to the bone response to mechanical loading where the area subjected to higher stress can develop more bone formation [50], thus results in a higher mineral-to-matrix ratio or more collagen fiber in the osteon. Further study could be conducted to examine the composition of the single osteon in porcine femur and tibia to gain more understanding in this mechanism of higher mechanical properties in the femur.

5.5 LIMITATION AND PROSPECT

There are several limitations for this study. Firstly, the amount of samples is not enough and thus the result can be more representative if greater number of sample were tested. Also, testing was conducted under dehydrated condition, while natural biological tissue is

normally wet. It is known that the sample hardens when it dehydrates [41], and the degree of hardening depends on the tested bone structure and the testing direction [7]. For example, osteon had a 42% increase while the interstitial bone 26% from wet to dry sample. In addition, there is no comprehensive study drawing the drying effect between the tibia and femur in the porcine bone. To further understand the in vivo mechanical properties in different regions and bones, this part of research would be crucial in the future in order to bridge the gap for differences of the properties between dry and wet samples.

Nevertheless, this study provides an overall measurement of the porcine femoral and tibial bones, including the regional effect (anterior to posterior) and direction effect. This information can be a step further for the study for the biomechanics of the porcine extremity. Finally, since pig bone has a certain degree similarity to the human bone [42], it may become the groundwork for studying human biomechanics, contributing to the knowledge of human bone disease.

Table 5: Locations having significant differences in measure values between areas (marked by X).

	Er	H
1FemurXA		
1FemurXP		
1FemurY		
1FemurZ		
1TibiaXA		
1TIbiaXP		
1TibiaY		
1TibiaZ		
2FemurXA		
2FemurXP		X
2FemurY		
2FemurZ	X	
2TibiaXA	X	
2TibiaXP	X	
2TibiaY	X	X
2TibiaZ		
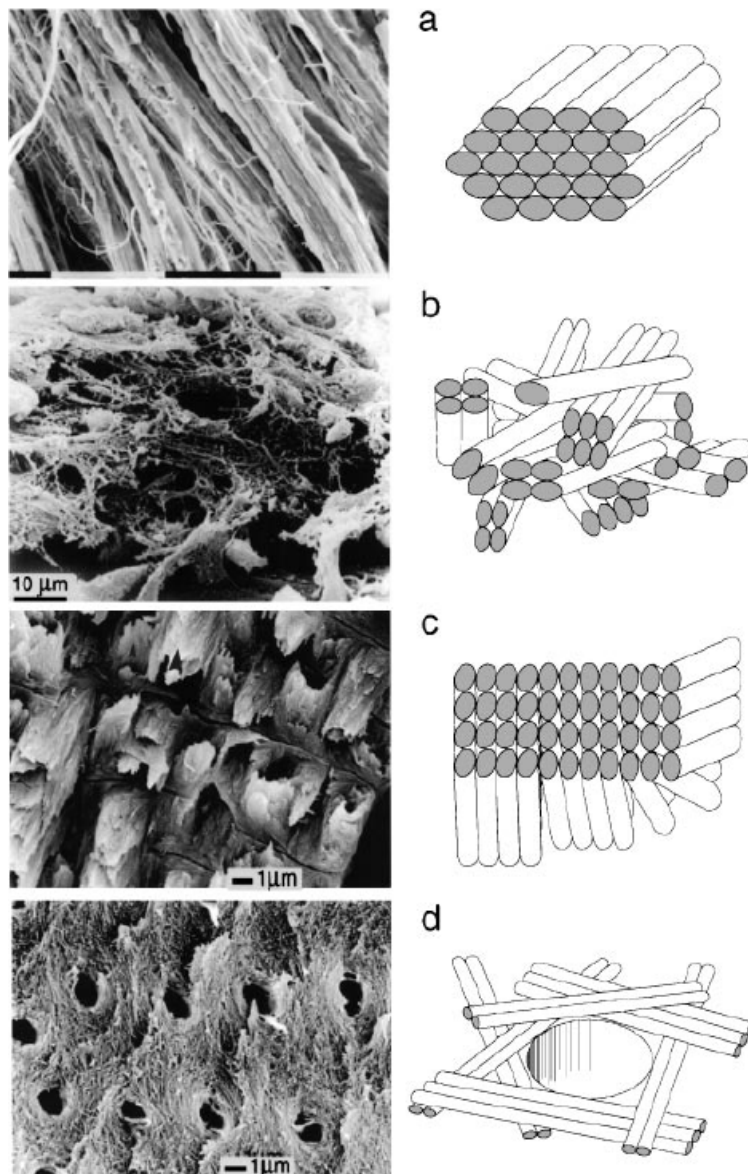
Figure 6 Four of the most common fibril array patterns of organization. SEM micrographs of fractured surfaces and schematic illustrations (not drawn to scale) of the basic organizational motifs. (*a*) Array of parallel fibrils. SEM: mineralized turkey tendon (scale: 0.1 mm). Schematic illustration showing the localized orthotropic symmetry of a fibril bundle. (*b*) Woven fiber structure. SEM: outer layer of a 19-week old human fetus femur. (Micrograph provided by X Su. Also published in Reference 52.) Schematic illustration showing fibril bundles with varying sized diameters arranged in different orientations. (*c*) Plywood-like structure present in lamellar bone. SEM: fracture surface of a baboon tibia showing the prominent fourth (*large arrowhead*) and fifth (*small arrowhead*) sub-layers (63, 72). Schematic illustration showing the five sub-layer model described in (63) with sub-layers one (*right hand side*), two, and three arbitrarily composed of one fibril layer each, whereas sub-layers four and five are composed of four fibril layers each. Note that the fibrils in each layer are rotated relative to their neighbors (depicted by the change in direction of the ellipsoid cross-section), following the rotated plywood model (67). (*d*) Radial fibril arrays. SEM: human dentin fractured roughly parallel to the pulp cavity surface. The tubules (*holes*) are surrounded by collagen fibrils that are all more or less in one plane. Schematic illustration of the fibril bundles arranged in a plane perpendicular to the tubule long axis. Within the plane they have no obvious preferred orientation.

Figure 38: SEM images and sketches of four types structures from Weiner & Wagner [40].

APPENDIX A

MECHANICAL PROPERTIES OF EACH AREA

The bar charts and tables in the next pages are a summary of the data from the testing. Figure 39 is the mechanical properties in each area of the pig1 and Figure 40 is the mechanical properties in each area of the pig2. Different regions are divided into groups by the vertical black lines. Table 6 lists the numerical values of reduced modulus and hardness at each area of both animals. The numbers of areas in the bone are given in Table 1.
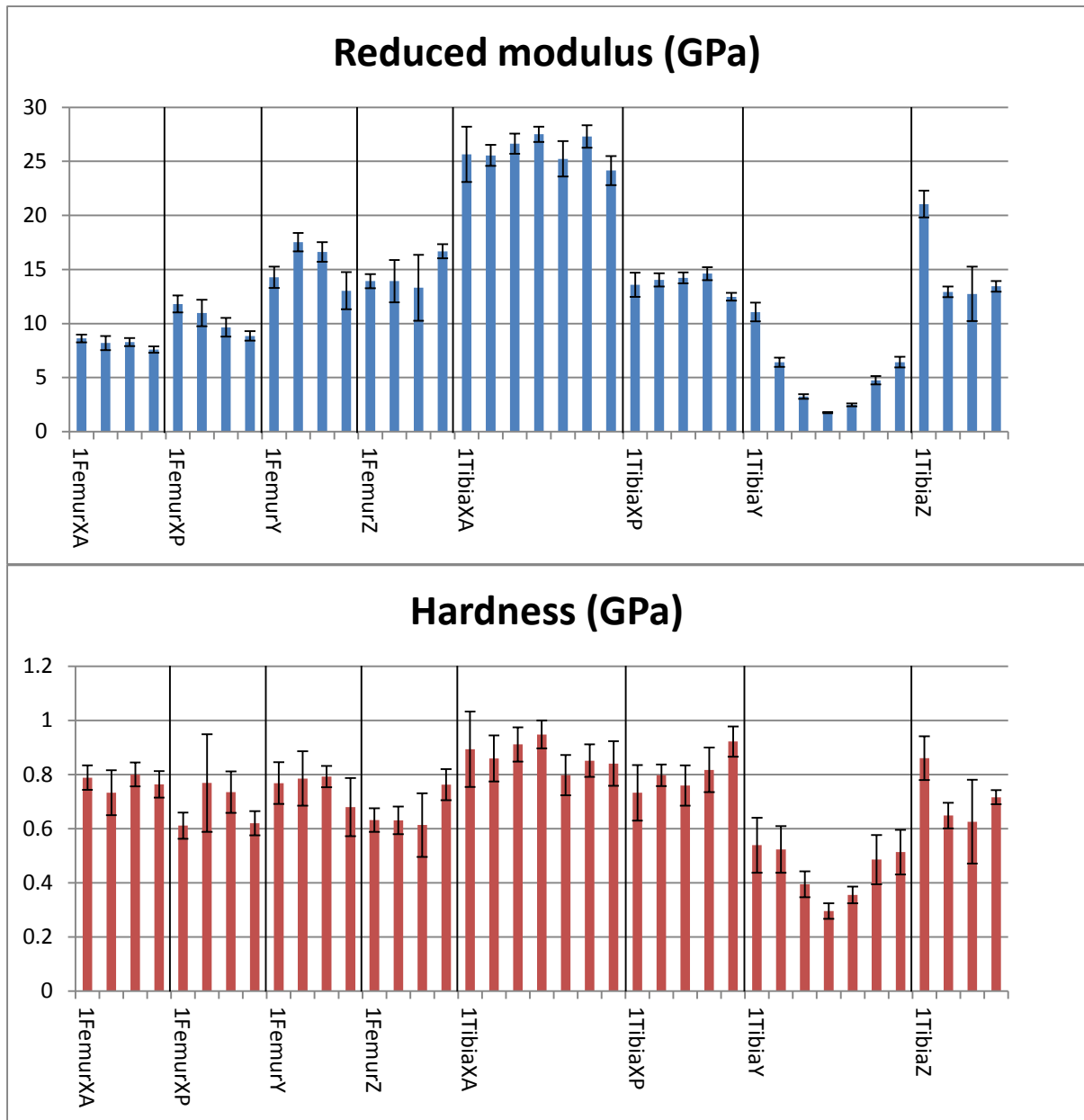
Figure 39: Mechanical properties at each area in pig1.
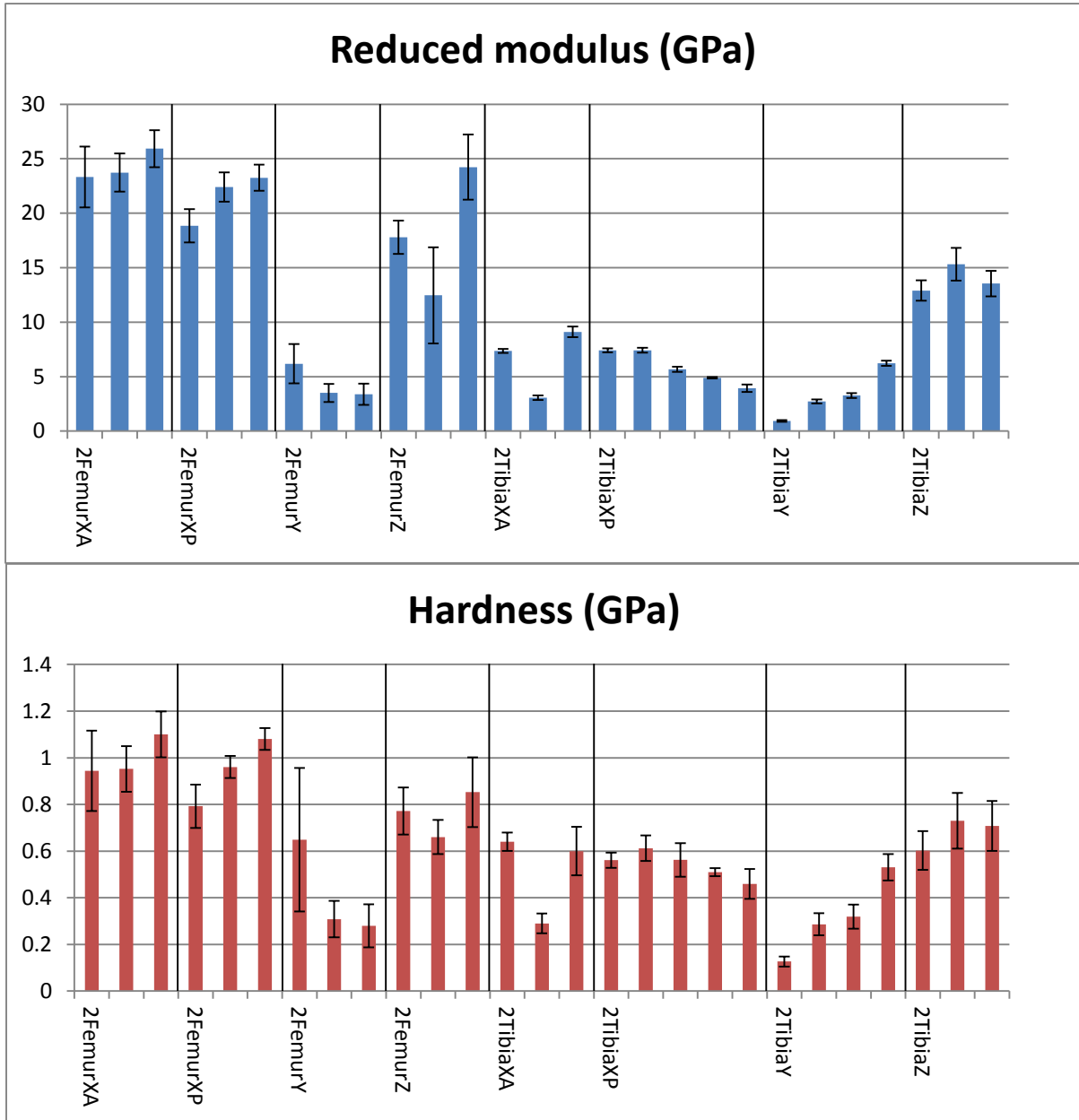
Figure 40: Mechanical properties at each area in pig2.

Table 6: Mechanical properties at each area

	Area	Reduced modulus (GPa)	Er-Standard deviation	Hardness (GPa)	H-Standard deviation
1FemurXA	1	8.621115	0.360116	0.7887281	0.045367
	2	8.194665	0.643193	0.7331334	0.082695
	3	8.285499	0.370904	0.8000397	0.044104
	4	7.594873	0.30297	0.7639219	0.048757
1FemurXP	1	11.81398	0.775532	0.6114419	0.048294
	2	10.9775	1.23164	0.7688363	0.180057
	3	9.654228	0.865754	0.7351296	0.076432
	4	8.848215	0.439543	0.6204034	0.044947
1FemurY	1	14.27434	0.988857	0.7684679	0.077422
	2	17.52562	0.862449	0.78554	0.100447
	3	16.61433	0.903751	0.7920844	0.039396
	4	13.03751	1.707413	0.6796963	0.107539
1FemurZ	1	13.92495	0.648372	0.6321654	0.04383
	2	13.92508	1.963974	0.6303937	0.051066
	3	13.30963	3.053773	0.613337	0.117242
	4	16.68336	0.64695	0.7626301	0.057128
1TibiaXA	1	25.65433	2.56066	0.8932978	0.139538
	2	25.55018	0.969125	0.8595382	0.084769
	3	26.63694	0.93231	0.9114636	0.063366
	4	27.50196	0.695949	0.9482578	0.052015
	5	25.2326	1.635832	0.7977336	0.07472
	6	27.30113	1.031468	0.8511912	0.060096
	7	24.15438	1.347959	0.8407162	0.082193
1TibiaXP	1	13.58422	1.11757	0.732867	0.10259
	2	14.0378	0.604911	0.7974058	0.040152
	3	14.21862	0.509739	0.7593782	0.074846
	4	14.61875	0.597952	0.8172262	0.082399
	5	12.47657	0.367019	0.9219338	0.055743
1TibiaY	1	11.06206	0.871433	0.538991	0.101716
	2	6.430766	0.424664	0.5234036	0.085672
	3	3.253294	0.209208	0.3946534	0.048193
	4	1.765637	0.061691	0.2959126	0.029027
	5	2.486085	0.135356	0.3550994	0.030591
	6	4.756894	0.376251	0.485883	0.090798
	7	6.430589	0.488355	0.5136496	0.082364

Table 6 (continued)

1TibiaZ	1	21.05226	1.23758	0.860273	0.080648
	2	12.93179	0.486651	0.6486736	0.047263
	3	12.73523	2.515482	0.6257426	0.154796
	4	13.44049	0.482807	0.7161172	0.026105
2FemurXA	1	23.3236	2.783753	0.943728	0.172462
	2	23.7289	1.752368	0.952375	0.09785
	3	25.92176	1.706185	1.099916	0.098336
2FemurXP	1	18.8472	1.529432	0.792457	0.09309
	2	22.40834	1.340493	0.960519	0.047764
	3	23.25365	1.197298	1.080612	0.046698
2FemurY	1	6.185081	1.809618	0.648556	0.307677
	2	3.508142	0.826228	0.308247	0.078601
	3	3.374453	0.973323	0.279363	0.092445
2FemurZ	1	17.79433	1.537087	0.771488	0.100764
	2	12.45721	4.418024	0.66026	0.073567
	3	24.22495	2.989146	0.852571	0.149741
2TibiaXA	1	7.362357	0.177483	0.640261	0.038992
	2	3.062179	0.20675	0.289396	0.042454
	3	9.106778	0.481122	0.599755	0.104057
2TibiaXP	1	7.412138	0.188373	0.56075	0.032884
	2	7.424591	0.229318	0.61231	0.055185
	3	5.664456	0.233827	0.562304	0.071872
	4	4.892688	0.076036	0.50962	0.017283
	5	3.937769	0.342049	0.459173	0.064403
2TibiaY	1	0.924124	0.082297	0.126546	0.021535
	2	2.718596	0.189259	0.285949	0.047099
	3	3.26665	0.230499	0.319116	0.051983
	4	6.22862	0.236135	0.53007	0.056685
2TibiaZ	1	12.90154	0.9303	0.602042	0.082952
	2	15.31328	1.50649	0.729692	0.119141
	3	13.53928	1.162609	0.708068	0.106881

APPENDIX B

TUKEY TEST- COMPARISON OF DATA FROM DIFFERENT AREAS

The Tukey test was used to compare sets of data, which were measured in different areas of a specific region. For example, for a region of bone where four areas were tested, the Tukey test compares area1 to area2, area1 to area3, area1 to area4, area2 to area3, area2 to area4 and area3 to area4. Table 7 gives the comparisons of properties between areas in the same region. Figure 41, Figure 42 and Figure 43 give the p values for comparison between areas in the femur and tibia in pig1, respectively. Figure 44 and Figure 45 give the p values for comparisons between areas in the femur and tibia in pig2, respectively. The red horizontal line indicates the p=0.05, so the bar over this line means p>0.05 and there is no significant difference in this comparison.

Table 7: P values for the comparison between areas in the same region.

			P value	
			Er	H
1	FemurXA	2-1	0.291	0.2937
		3-1	0.4946	0.9825
		4-1	0.0011	0.8504
		3-2	0.9799	0.1583
		4-2	0.0768	0.7497
		4-3	0.0338	0.6477
	FemurXP	2-1	0.9907	0.9992
		3-1	0	0.3688
		4-1	0	0.9053
		3-2	0	0.4405
		4-2	0	0.9475
		4-3	0.1564	0.7627
	FemurY	2-1	0.0001	0.9818
		3-1	0.0051	0.9542
		4-1	0.2227	0.2371
		3-2	0.4761	0.9989
		4-2	0	0.122
		4-3	0	0.0924
	FemurZ	2-1	1	1
		3-1	0.9263	0.9628
		4-1	0.0502	0.014
		3-2	0.9263	0.9719
		4-2	0.0503	0.0126
		4-3	0.0126	0.0045
1	TibiaXA	2-1	1	0.9949
		3-1	0.928	0.9998
		4-1	0.4157	0.9411
		5-1	0.9991	0.5589
		6-1	0.5495	0.9838
		7-1	0.6508	0.952
		3-2	0.8891	0.9547
		4-2	0.3524	0.6397
		5-2	0.9998	0.9016
		6-2	0.4786	1
		7-2	0.7202	0.9998
		4-3	0.9598	0.992

Table 7 (continued)

		5-3	0.7147	0.3572
		6-3	0.9893	0.9115
		7-3	0.1261	0.831
		5-4	0.1972	0.1033
	TibiaXA	6-4	1	0.5412
		7-4	0.0148	0.4219
		6-5	0.2883	0.9482
		7-5	0.8927	0.982
		7-6	0.0252	1
1		2-1	0.8328	0.6511
		3-1	0.5996	0.9788
		4-1	0.1625	0.404
		5-1	0.1199	0.0054
	TibiaXP	3-2	0.9932	0.9249
		4-2	0.6735	0.9929
		5-2	0.0141	0.0988
		4-3	0.886	0.7344
		5-3	0.0056	0.0187
		5-4	0.0007	0.2104
1	TibiaY	2-1	0	0.9999
		3-1	0	0.0529
		4-1	0	0.0002
		5-1	0	0.0066
		6-1	0	0.9038
		7-1	0	0.9976
		3-2	0	0.1094
		4-2	0	0.0006
		5-2	0	0.0155
		6-2	0	0.981
		7-2	1	1
		4-3	0.0002	0.3515
		5-3	0.1286	0.9753
		6-3	0.0002	0.4432
		7-3	0	0.1659
		5-4	0.1769	0.8505
		6-4	0	0.0047
		7-4	0	0.001
		6-5	0	0.0999

Table 7 (continued)

1	TibiaY	7-5	0	0.0259
		7-6	0	0.9961
	TibiaZ	2-1	0	0.0102
		3-1	0	0.0045
		4-1	0	0.0989
		3-2	0.9963	0.9781
		4-2	0.9432	0.655
		4-3	0.8656	0.4252
2	FemurXA	2-1	0.9426	0.9925
		3-1	0.1227	0.1198
		3-2	0.2113	0.1465
	FemurXP	2-1	0.0014	0.0019
		3-1	0.0003	0
		3-2	0.5791	0.027
	FemurY	2-1	0.0095	0.0239
		3-1	0.0092	0.0192
		3-2	0.983	0.964
	FemurZ	2-1	0.0288	0.2332
		3-1	0.0089	0.4446
		3-2	0	0.0249
2	TibiaXA	2-1	0	0
		3-1	0	0.631
		3-2	0	0
	TibiaXP	2-1	1	0.5195
		3-1	0	1
		4-1	0	0.5273
		5-1	0	0.0384
		3-2	0	0.6012
		4-2	0	0.0357
		5-2	0	0.0012
		4-3	0.0007	0.5542
		5-3	0	0.0504
		5-4	0	0.5399
	TibiaY	2-1	0	0.0004
		3-1	0	0.0002
		4-1	0	0
		3-2	0.0067	0.7529
		4-2	0	0

Table 7 (continued)

		4-3	0	0.0001
		2-1	0.0294	0.1978
	TibiaZ	3-1	0.6843	0.273
		3-2	0.1124	0.9473
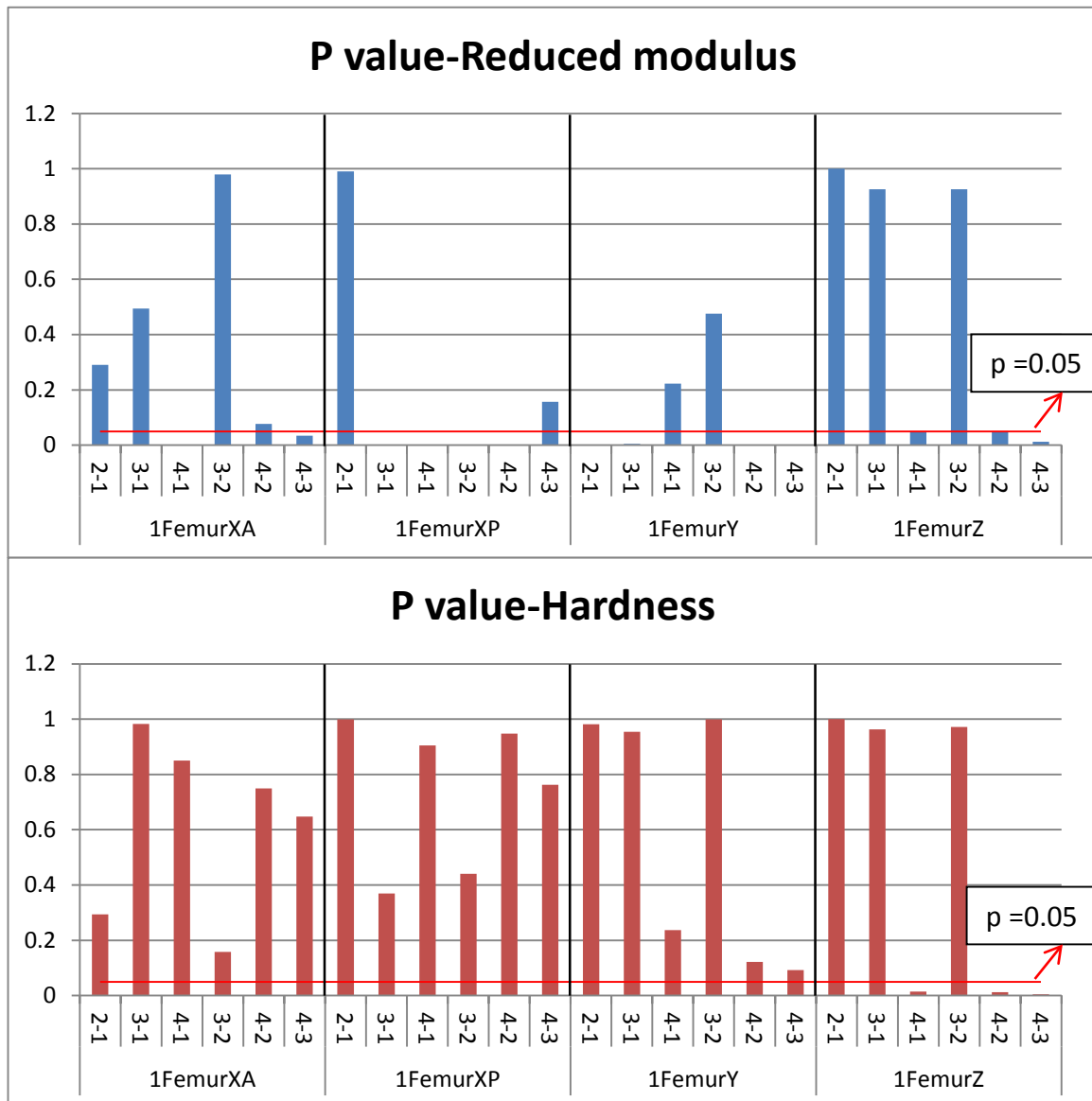
Figure 41: P values for the comparisons between areas in the femur in pig1. Note that the p value for the reduced modulus comparison of 1FemurZ 4-1 and 4-2 are 0.0502 and 0.0503 respectively, meaning there are no significant differences found in these two comparisons.
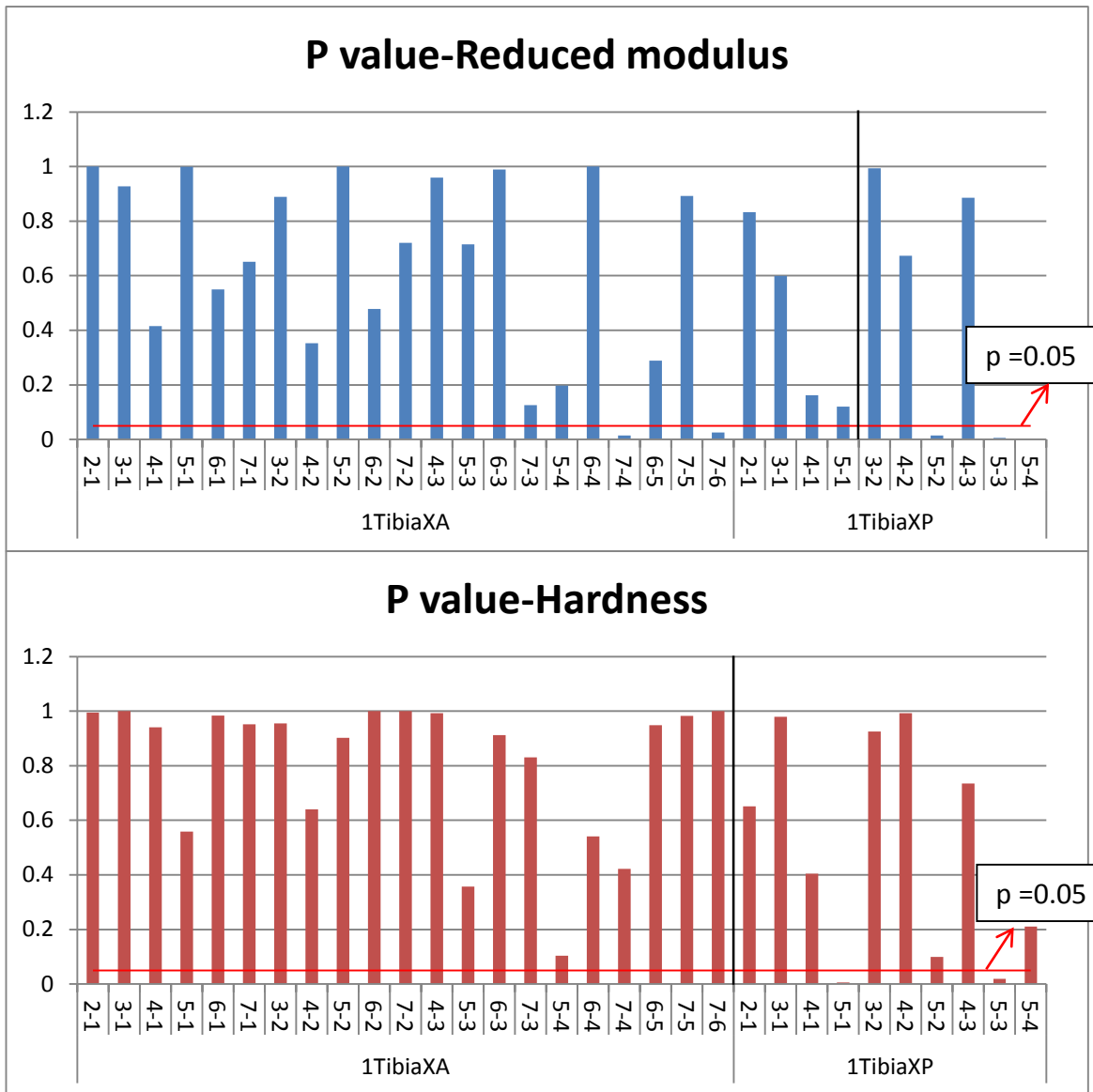
Figure 42: P values for comparisons between the anterior and posterior regions in the tibia of pig1.
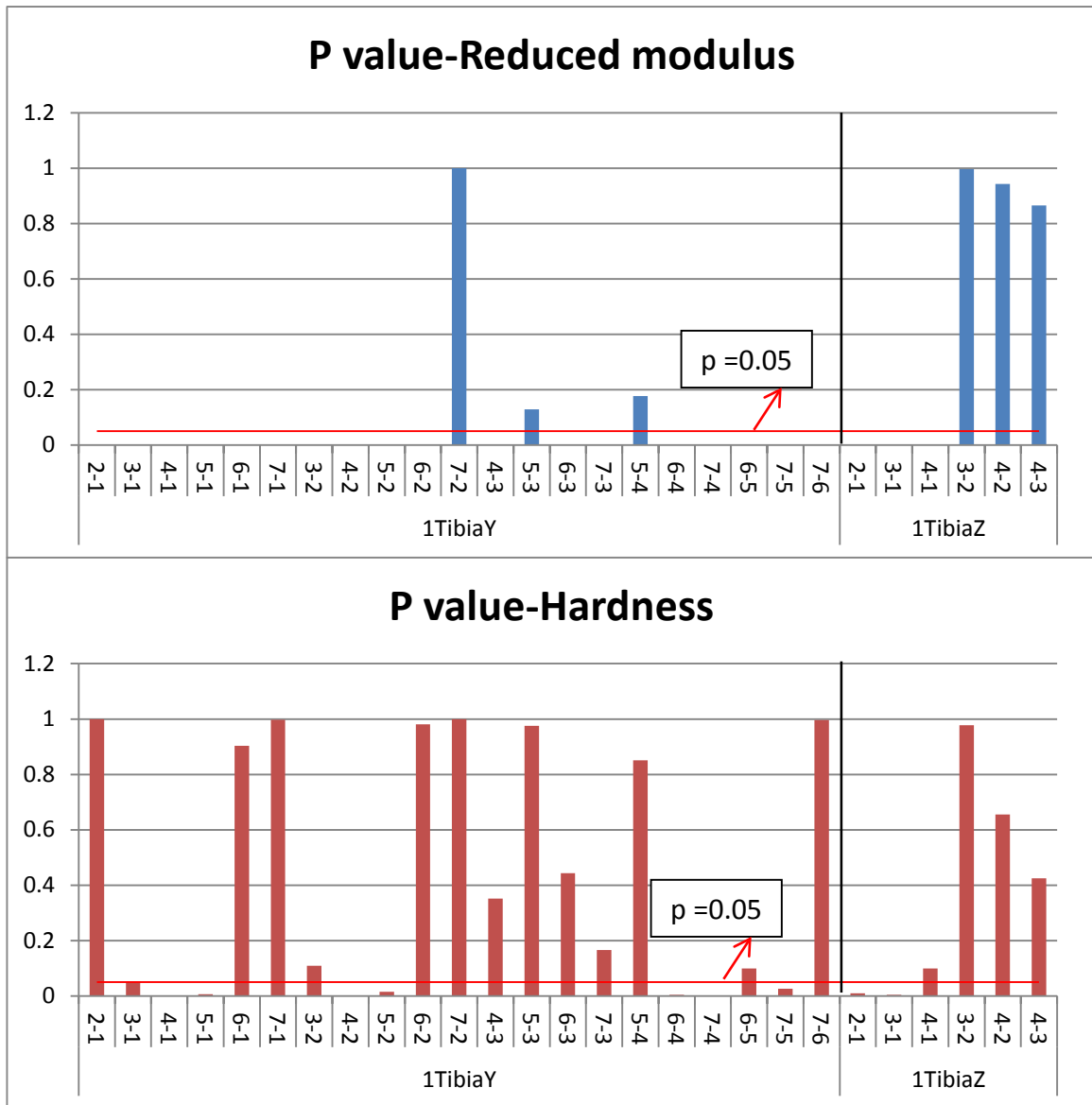
Figure 43: P values for the comparisons between properties in y and z directions in the tibia of pig1. Note that the p value of the hardness comparison for 1TibiaY 3-1 is 0.0529, meaning no significant difference found in this comparison.
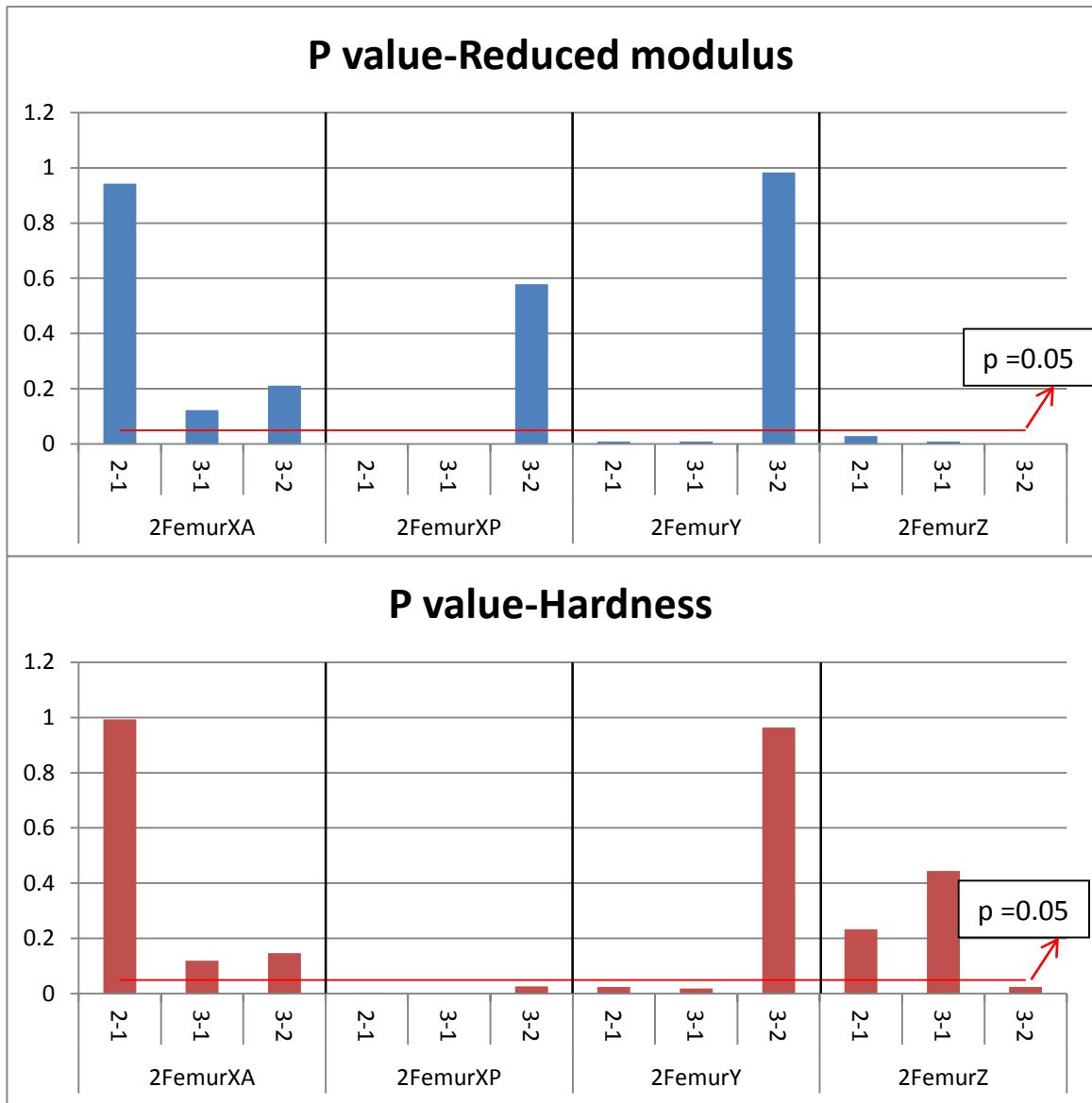
Figure 44: P values of comparison of material properties for the femur of pig2.
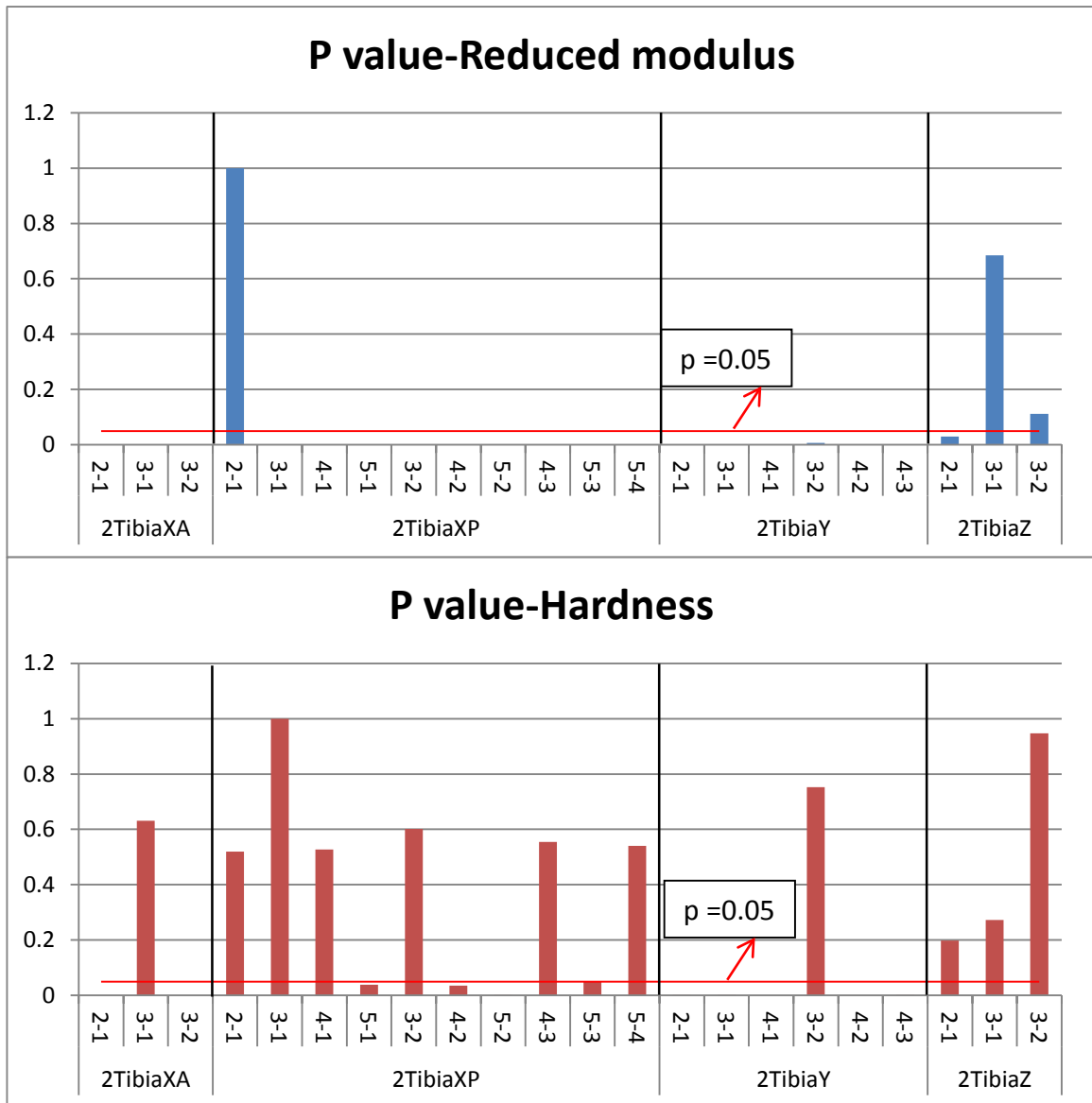
Figure 45: P values of comparison for the tibia of pig2. Note that the p value for the

hardness comparison of the 2TibiaXP 5-3 is 0.0504, meaning no significant difference found

in this comparison.

LINEAR MIXED MODEL

Table 8 shows the result from linear mixed model. The value column is used by Eq. (4) to convert back to the mean value of the mechanical properties.

Table 8: The raw data from linear mixed model for regional and bone effect.

Reduced modulus					
	Estimate	Std.Error	DF	t-value	p-value
Intercept	8.40891	1.01339	361	8.29782	0
Tibia (B_{Tibia})	-1.7843	0.66104	361	-2.6992	0.0073
Y (B_{DY})	7.55051	0.95625	361	7.89593	0
XA (B_{DXA})	9.76954	0.90803	361	10.7591	0
XP (B_{DXP})	4.55402	0.91435	361	4.98062	0
Hardness					
	Estimate	Std.Error	DF	t-value	p-value
Intercept	0.55574	0.03951	361	14.066	0
Tibia (B_{Tibia})	-0.1129	0.01771	361	-6.3757	0
Y (B_{DY})	0.1844	0.02563	361	7.19517	0
XA (B_{DXA})	0.30251	0.02433	361	12.4319	0
XP (B_{DXP})	0.22418	0.02451	361	9.14664	0

APPENDIX D

R CODE FOR LINEAR MIXED MODEL

```
data=read.table("C:\\Users\\goldsam\\Desktop\\All.txt")   # Data loaded

Y1=data[,1]                                               # Y1=the first column of data

Y2=data[,2]                                               # Y2=the second column of data

Pig=c(rep(1,times=227),rep(2,times=140))                 # Label data groups

Part=c(rep(1,times=112),rep(2,times=115),rep(1,times=69),rep(2,times=71))

Direction=c(rep(1,times=28),rep(2,times=28),rep(3,times=28),rep(4,times=28),

rep(1,times=35),rep(2,times=20),rep(3,times=35),rep(4,times=25),

rep(1,times=16),rep(2,times=18),rep(3,times=18),rep(4,times=17),

rep(1,times=18),rep(2,times=14),rep(3,times=15),rep(4,times=24))

PIG=as.factor(Pig)                                       # Take groups as factors

PART=as.factor(Part)

DIRECTION=as.factor(Direction)

summary(logisr<- lme(Y1~PART+DIRECTION, random=~1 | PIG))       #Do linear mixed
                                                                 model analysis

summary(logisr<- lme(Y2~PART+DIRECTION, random=~1 | PIG))
```

R CODE FOR TUKEY TEST

```
data=read.table("C:\\Users\\goldsam\\Desktop\\1FD.txt")        # Data loaded

ind=c(rep(1,times=28),rep(2,times=28),rep(3,times=56))    # Label data groups

y1=data[,1]                                              # y1=the first column of data

y2=data[,2]

result=aov(y1~as.factor(ind))                           #Do Tukey test

result=aov(y2~as.factor(ind))

anova(result)

TukeyHSD(result)

plot(TukeyHSD(result))
```

R CODE FOR ONE-WAY ANOVA

```
data=read.table("C:\\Users\\goldsam\\Desktop\\1FA to P.txt")# Data loaded

y1=data[,1]                                              # y1=the first column of data

ind1=c(rep(1,times=28),rep(0,times=28))                 # Label data groups

ind2=c(rep(0,times=28),rep(1,times=28))

summary(lm(y1~ind2))                                    #Do One-way ANOVA

summary(aov(y1~ind2))

y2=data[,2]

summary(aov(y2~ind2))
```

APPENDIX E

COMPARISON OF PROPERTIES OF BONE FOR PAST AND CURRENT STUDIES

Table 9 gives either the elastic or reduced modulus of bone measured by nanoindentation from previous studies mentioned in the background section and current study. Table 10 gives the hardness of bone measured by nanoindentation from previous studies in the background section and current study.

Table 9: Nanoindentation modulus measurement of bone.

Study	Specimen	E or Er(GPa)					
Giambini et al. [9]	Human vertebrae trabecular bone	T7		T8		L4	
		A	P	A	P	A	P
		19.8	17.8	19.6	18.8	17.6	17.5
Gupta et al. [11]	Human femoral cortical bone(Er)	Osteon			Interstitial bone		
		24~27			Er: >30		
Fan et al. [6]	Human tibial bone	Osteon			Interstitial bone		
		D11	D22	D33	D11	D22	D33
		16.6	17.0	25.1	19.7	18.5	27.1
Milovanovic et al. [16]	Human femoral trabecular bone	Young			Old		
		1.28			1.97		
Gourison-Arsiquaud et al. [10]	Baboon femoral cortical bone	Different tissue age					
		30~35					
Burket et al. [1]	Baboon femoral cortical bone	Different animal and tissue age					
		20~40					
Feng et al. [7]	Porcine femoral cortical bone		Interstitial		Osteon		Transverse osteon
		Wet	~20		~19		~15
		Dry	~25		~26		~26
Current study	Porcine femoral and tibial cortical bone(Er)		XA	XP		Y	Z
		Femur	7.5	13		8.2	18.2
		Tibia	16.1	11		6.5	14

Table 10: Nanoindentation hardness measurement of bone.

Study	Specimen	H(GPa)					
Giambini et al. [9]	Human vertebrae trabecular bone	T7		T8		L4	
		A	P	A	P	A	P
		0.74	0.74	0.74	0.73	0.64	0.65
Gupta et al. [11]	Human femoral cortical bone	No result					
Fan et al. [6]	Human tibial bone	No result					
Mi-lovanovic et al. [16]	Human femoral trabecular bone	Young			Old		
		0.59			0.92		
Gourison-Arsi-quaud et al. [10]	Baboon femoral cortical bone	Different tissue age					
		1.4~1.2					
Burket et al. [1]	Baboon femoral cortical bone	Different animal and tissue age					
		0.8~2.2					
Feng et al. [7]	Porcine femoral cortical bone		Interstitial		Osteon		Transverse osteon
		Wet	~0.7		~0.5		~0.6
		Dry	~1.0		~0.9		~1.1
Current study	Porcine femoral and tibial cortical bone		XA	XP		Y	Z
		Femur	0.85	0.78		0.55	0.74
		Tibia	0.75	0.68		0.44	0.61

BIBLIOGRAPHY

[1]   **Burket, J., et al.** Microstructure and nanomechanical properties in osteons related to tissue and animal age. *Journal of Biomechanics.* 2011, Vol. 44, pp. 277-284.

[2]   **Ebenstein, D.M.** A comparison of JKR-based methods to analyze quasi-static and dynamic indentation force curves. *Journal of Materials Research.* 2011, Vol. 26, pp. 1026-1035.

[3]   **Ebenstein, D.M. and Pruitt, L.A.** Nanoindentation of biological materials. *Nanotoday.* 2006, Vol. 1, pp. 26-33.

[4]   **Ebenstein, D.M. and Pruitt, L.A.** Nanoindentation of soft hydrated materials for application to vascular tissues. *Journal of Biomedical Materials Research.* A, 2004, Vol. 69, pp. 222-232.

[5]   **Ebenstein, D.M. and Wahl, K.J.** A comparison of JKR-based methods to analyze quasi-static and dynamic indentation force curves. *Journal of Colloid and Interface Science.* 2006, Vol. 298, pp. 652-662.

[6]   **Fan, Z., et al.** Anisotropic properties of human tibial cortical bone as measured by nanoindentation. *Journal of Orthopaedic Research.* 2002, Vol. 20, pp. 806-810.

[7]   **Feng, L., et al.** Mechanical properties of porcine femoral cortical bone measured by nanoindentation. *Journal of Biomechanics.* 2012, Vol. 45, pp. 1775-1782.

[8]   **Franke, O., Göken, M. and Hodge, A.M.** The nanoindentation of soft tissue: Current and developing approaches. *JOM.* 2008, Vol. 60, pp. 49-53.

[9]   **Giambini, H., et al.** Anterior and posterior variations in mechanical properties of human vertebrae measured by nanoindentation. *Journal of Biomechanics.* 2013, Vol. 46, pp. 456-461.

[10]   **Gourion-Arsiquaud, S., et al.** Spatial variation in osteonal bone properties relative to tissue and animal age. *Journal of Bone and Mineral Research.* 2009, Vol. 24, pp. 1271-1281.

[11] **Gupta, H.S., Stachewicz, U. and Wagermaier, W.** Mechanical modulation at the lamellar level in osteonal bone. *Journal of Materials Research.* 2006, Vol. 21, pp. 1913-1921.

[12] **Isaksson, H., et al.** Precision of nanoindentation protocols for measurement of viscoelasticity in cortical and trabecular bone. *Journal of Biomechanics.* 2010, Vol. 43, pp. 2410-2417.

[13] **Kaufman, J.D. and Klapperich, C.M.** Surface detection errors cause overestimation of the modulus in nanoindentation on soft materials. *Journal of the Mechanical Behavior of Biomedical Materials.* 2009, Vol. 2, pp. 312-317.

[14] **Ma, Q. and Clarke, D.R.** Size dependent hardness of silver single crystals. *Journal of Materials Research.* 1995, Vol. 10, pp. 853-863.

[15] **Meerbeek, B.V., et al.** Assessment by nanoindentation of the hardness and elasticity of the resin-dentin bonding area. *Journal of Dental Research.* 1993, Vol. 72, pp. 1434-1442.

[16] **Milovanovic, P., et al.** Age-related deterioration in trabecular bone mechanical properties at material level: Nanoindentation study of the femoral neck in women by using AFM. *Experimental Gerontology.* 2012, Vol. 47, pp. 154-159.

[17] **Oliver, W.C. and Pharr, G.M.** An improved technique for determining hardness and elastic modulus using load and displacement sensing indentation experiments. *Journal of Materials Research.* 1992, Vol. 7, pp. 1564-1583.

[18] **Paietta, R.C., Campbell, S.E. and Ferguson, V.L.** Influences of spherical tip radius, contact depth, and contact area on nanoindentation properties of bone. *Journal of Biomechanics.* 2011, Vol. 44, pp. 285-290.

[19] **Rettler, E., et al.** Mapping the mechanical properties of biomaterials on different length scales: Depth-sensing indentation and AFM based nanoindentation. *Journal of Materials Chemistry.* B, 2013, Vol. 1, pp. 2789-2806.

[20] **Rho, J.Y., Kuhn-Spearing, L. and Zioupos, P.** Mechanical properties and the hierarchical structure of bone. *Medical Engineering and Physics.* 1998, Vol. 20, pp. 92-102.

[21] **Rho, J.Y., Tsui, T.Y. and Pharr, G.M.** Elastic properties of human cortical and trabecular lamellar bone measure by nanoindentation. 1997, Vol. 18, pp. 1325-1330.

[22] **Saha, R. and Nix, W.D.** Effects of the substrate on the determination of thin film mechanical properties by nanoindentation. *Acta Materialia.* 2002, Vol. 50, pp. 23-38.

[23] **Wu, Z., et al.** The effect of holding time on nanoindentation measurements of creep in bone. *Journal of Biomechanics.* 2011, Vol. 44, pp. 1066-1072.

[24] **Peng, Z., Gong, J. and Miao, H.** On the description of indentation size effect in hardness testing for ceramics: Analysis of the nanoindentation data. *Journal of the European Ceramic Society.* 2004, Vol. 24, pp. 2193-2201.

[25] **Zhou, J., Hsiung, L.L.** Depth-dependent mechanical properties of enamel by nanoindentation. *Journal of Biomedical Materials Research.* A, 2007, Vol. 81, pp. 66-74.

[26] **Rho, J.Y., Zioupos, P., Currey, J.D., Pharr, G.M.** Microstructural elasticity and regional heterogeneity in aging human bone examined by nanoindentation. *Journal of Biomechanics.* 2002, Vol. 35, pp. 161-165.

[27] **Swadener, J.G.. Pharr, G.M.** Indentation of elastically anisotropic half-spaces by cones and parabolas of revolution. *Philosophical Magazine.* A, 2001, Vol. 81, pp. 447-466.

[28] **Swadener, J.G., Rho, J.Y., Pharr, G.M.** Effects of anisotropy on elastic moduli measured by nanoindentation in human tibial cortical bone. *Journal Biomedical Materials Research.* 2001, Vol. 57, pp. 108-112.

[29] **Guidoni, G., Swain, M., Jager, I.** Nanoindentation of wet and dry compact bone: Influence of environment and indenter tip geometry on the indentation modulus. *Philosophical Magazine.* 2010, Vol. 90, pp. 553-565.

[30] **Donnelly,E., Baker, S.P., Boskey, A.L., van der Meulen, M.C.H.** Effects of surface roughness and maximum load on the mechanical properties of cancellous bone measured by nanoindentation. *Journal of Biomedical Materials Research.* A, 2006, Vol. 77, pp. 425-435

[31] **Rho, J.Y., Pharr, G.M.** Effects of drying on the mechanical properties of bovine femur measured by nanoindentation. *Journal of Material Science: Materials in Medicine.* 1999, Vol. 10, pp. 485-488.

[32] **Zhang, J.Z., Michalenko, M.M., Kuhl, E., Ovaert, T.C.** Characterization of indentation response and stiffness reduction of bone using a continuum damage model. *Journal of the Mechanical Behavior of Biomedical Materials.* 2010, Vol. 3, pp. 189-202.

[33] **Barak, M.M., Lieberman, D.E., Hublin, J.** A Wolff in sheep's clothing: trabecular bone adaptation in response to changes in joint loading orientation. *Bone.* 2011, Vol. 49, pp. 1141-1151.

[34] **Rubin, C.T., Lanyon, L.E.** Regulation of bone mass by mechanical strain magnitude. *Calcified Tissue International.* 1985, Vol. 37, pp. 411-417.

[35] **FranZoso, G., Zysset, P.K.** Elastic anisotropy of human cortical bone secondary osteons measure by nanoindentation. *Journal of Biomechanical Engineering.* 2009, Vol. 131, pp. 021001-1-021001-11

[36] **Reisinger, A.G., Pahr, D.H., Zysset, P.K.** Elastic anisotropy of bone lamellae as a function of fibril orientation pattern. *Biomechanics and Modeling in Mechanobiology.* 2011, Vol. 10, pp. 67-77

[37] **Rho, J.Y., Currey, J.D., Zioupos, P., Pharr, G.M.** The anisotropic Young's modulus of equine secondary osteons and interstitial bone determined by nanoindentation. *Journal of Experimental Biology.* 2001, Vol. 204, 1775-1781.

[38] **Liu, D., Wagner, H.D., Weiner, S.** Bending and fracture of compact circumferential and osteonal lamellar bone of the baboon tibia. *Journal of Material Science: Materials in Medicine.* 2000, Vol. 11, pp. 49-60.

[39] **Weiner, S., Arad, T., Sabanay, I., Traub, W.** Rotated plywood structure of primary lamellar bone in the rat: Orientations of the collagen fibril arrays. *Bone.* 1997, Vol. 20, pp. 509-514.

[40] **Weiner, S., Wagner, H.D.** The material bone: Structure-mechanical function relations. Annual Review of Material Science. 1998, Vol. 28, pp. 271-298.

[41] **Lewis, G., Nyman, J.S.** The use of nanoindentation for characterizing the properties of mineralized hard tissue: State-of-the art review. *Journal of Biomedical Materials Research: Applied Biomaterials.* B, 2008, Vol.87, pp. 286-301.

[42] **Pearce, A.I., Richards A.O., Milz, S., Schneider, E., Pearce, S.G.** Animal models for implant biomaterial research in bone: A review. *European Cells and Materials.* 2007, Vol. 13, pp. 1-10.

[43] **Bonney, H., Colston, B.J., Goodman, A.M.** Regional variation in the mechanical properties of cortical bone from the porcine femur. *Medical Engineering and Physics.* 2011, Vol. 33, pp. 513-520.

[44] **Currey, J.D.** What determines the bending strength of compact bone? *Journal of Experimental Biology*. 1999, Vol. 202, pp. 2495-2503.

[45] **Roe, S.C., Pijanowski, G.J., Johnson, A.L.** Biomechanical properties of canine cortical bone allografts: effects of preparation and storage. *American Journal of Veterinary Research*. 1988, Vol. 49, pp. 873-877

[46] **Panjabi, M.M., Krag, M., Summers, D., Videman, T.** Biomechanical time-tolerance of fresh cadaveric human spine specimens. *Journal of Orthopaedic Research.* 1985, Vol. 3, pp. 292-300.

[47] **Kang, Q., An, Y.H., Friedman, R.J.** Effects of multiple freezing-thawing cycles on ultimate indentation load and stiffness of bovine cancellous bone. *American Journal of Veterinary Research.* 1997, Vol. 58, pp. 1171-1173.

[48] **Riggs, C.M., Vaughan, L.C., Evans, G.P., Lanyon, L.E., Boyde, A.** Mechanical implications of collagen fibre orientation in cortical bone of the equine radius. *Anatomy and Embryology.* 1993, Vol. 187, pp. 239-248.

[49] **Currey, J.D.** The design of mineralized hard tissues for their mechanical functions. *Journal of Experimental Biology.* 1999, Vol. 202, pp. 3285-3294.

[50] **Turner, H.C., Robling, A.G.** Mechanisms by which exercise improves bone strength. *Journal of Bone and Mineral Metabolism.* 2005, Vol. 23, pp. 16-22.

[51] **Sisson, S., Grossman, J.D.** Anatomy of the domestic animals. 1953, (4th ed. (rev.)), WB Saunders., Philadelphia.

[52] **Stilwell, N.A., Tabor, D.** Elastic recovery of conical indentations. *Proceeding of the Physical Society.* 1961, Vol. 78, pp. 169-179

[53] **Doerner, M.F., Nix, W.D.** A method for interpreting the data from depth-sensing indentation instruments. *Journal of Materials Research*. 1986, Vol. 1, pp. 601-609.

[54] **Sneddon, I.N.** The relation between load and penetration in the axisymmetric boussinesq problem for a punch of arbitrary profile. *International Journal of Engineering Science.* 1965, Vol. 3, pp.47-57.

[55] **Harding, J.W., Sneddon, I.N.** The elastic stresses produced by the indentation of the plane surface of a semi-infinite elastic by a rigid punch. *Mathematical Proceedings of the Cambridge Philosophical Society.* 1945, Vol. 45, pp. 16-26.